

# PaGoDA : Progressive Growing of a One-Step Generator from a Low-Resolution Diffusion Teacher

**Dongjun Kim**\*<sup>†</sup>  
Stanford University  
CA, USA  
dongjun@stanford.edu

**Chieh-Hsin Lai**\*  
Sony AI  
Tokyo, Japan  
chieh-hsin.lai@sony.com

**Wei-Hsiang Liao**  
Sony AI

**Yuhta Takida**  
Sony AI

**Naoki Murata**  
Sony AI

**Toshimitsu Uesaka**  
Sony AI

**Yuki Mitsufuji**  
Sony AI, Sony Group Corporation

**Stafano Ermon**  
Stanford University

## Abstract

To accelerate sampling, diffusion models (DMs) are often distilled into generators that directly map noise to data in a single step. In this approach, the resolution of the generator is fundamentally limited by that of the teacher DM. To overcome this limitation, we propose **Progressive Growing of Diffusion Autoencoder (PaGoDA)**, a technique to progressively grow the resolution of the generator beyond that of the original teacher DM. Our key insight is that a pre-trained, low-resolution DM can be used to deterministically encode high-resolution data to a structured latent space by solving the PF-ODE forward in time (data-to-noise), starting from an appropriately down-sampled image. Using this frozen encoder in an auto-encoder framework, we train a decoder by progressively growing its resolution. From the nature of progressively growing decoder, PaGoDA avoids re-training teacher/student models when we upsample the student model, making the whole training pipeline much cheaper. In experiments, we used our progressively growing decoder to upsample from the pre-trained model’s  $64^2$  resolution to generate  $512^2$  samples, achieving  $2\times$  faster inference compared to single-step distilled Stable Diffusion like LCM [1]. PaGoDA also achieved state-of-the-art FIDs on ImageNet across all resolutions from  $64^2$  to  $512^2$ . Additionally, we demonstrated PaGoDA’s effectiveness in solving inverse problems and enabling controllable generation.

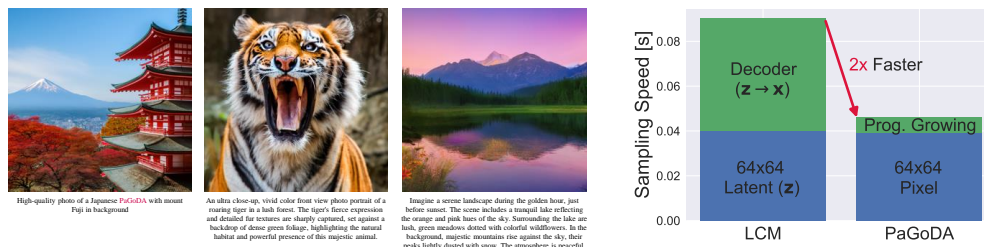


Figure 1: PaGoDA is a one-step generator faster than LCM [1], see more samples in Figures 8 and 15.

\*Equal contribution

<sup>†</sup>Work partially done during an internship at Sony AI

# 1 Introduction

Diffusion Models (DMs) [2, 3] have demonstrated remarkable generative capabilities. However, unlike models that directly map noise to data [4, 5], DMs adopt an incremental data generation process, equivalent to solving the so-called probability flow ordinary differential equation (PF-ODE) [3], inherently limiting their sample generation speed. To address this challenge, distilled DMs [6–8] have emerged as an alternative. These models are trained using a pre-trained DM acting as the teacher model, enabling fast generation by moving along the PF-ODE (from noise to denoised samples) through long jumps.

In distillation, the performance of distillation models is inherently constrained by that of the teacher model. Moreover, the teacher-student framework requires that the student model’s resolution exactly matches that of the teacher DM. Therefore, it is not possible to create a distilled student model that can generate higher resolutions than its teacher without training a new high-resolution teacher DM – a process that is particularly resource-intensive, especially for large-scale models and datasets.

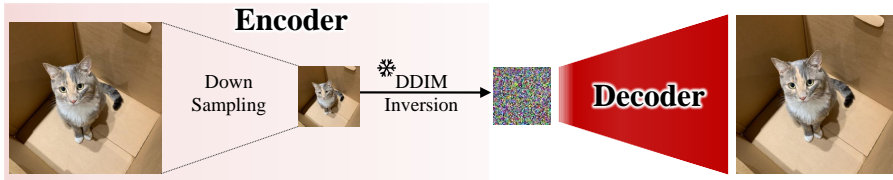


Figure 2: Model overview. PaGoDA constructs the encoder with downsampling followed by solving a pre-trained PF-ODE, and the docoder in a progressively growing manner for scalable generation.

To address these limitations, we take inspiration from the Progressive Growing GAN (PG GAN) [9], which gradually expands the generator architecture (freezing previously trained parts), enabling efficient scaling-up to high-resolutions. Building upon this insight, we introduce **Progressive Growing of Diffusion Autoencoder (PaGoDA)**. Our model utilizes a DM pre-trained on a base resolution as a frozen encoder in an AutoEncoder (AE) framework. Specifically, as illustrated in Figure 2, regardless of the input resolution, PaGoDA downsamples the input to the base resolution (compatible with the pre-trained DM), and solves its PF-ODE [3, 10] from time 0 to  $T$  to deterministically obtain a latent vector (e.g., via DDIM inversion [10, 11]). This downsampled latent is then fed into the decoder, which is trained to reconstruct the original input in a progressive growing manner. Compared to Stable Diffusion (SD) [12] and its distilled versions [13], we highlight PaGoDA’s features as follows:

**Progressively Growing Decoder:** PaGoDA’s direct pixel space training facilitates easy scalability for super resolution generation, achieving single-step generation  $2\times$  faster than distilled SD by bypassing decoding latents back to the pixel space.

PaGoDA achieves state-of-the-art (SOTA) Fréchet Inception Distance (FID) [14] on ImageNet [15] across different resolutions by distilling from a teacher model with a base resolution of  $64^2$ . Additionally, we extend PaGoDA to support Classifier-Free Guidance (CFG) [16], achieving competitive results in text-to-image (T2I) single-step generation. Furthermore, we demonstrate PaGoDA’s applicability in solving inverse problems and enabling controllable generation.

## 2 Preliminary and Related Works

DM [2, 3] samples from the data distribution  $p_{\text{data}}$  through an iterative denoising process, beginning from a Gaussian prior distribution  $p_{\text{prior}}$ . This denoising process attempts to reverse a fixed (forward) diffusion process. The deterministic counterpart of the denoising (generation) process, known as the probability flow ordinary differential equation (PF-ODE) [3, 10], is expressed as

$$\frac{d\mathbf{x}_t}{dt} = -t\nabla \log p_t(\mathbf{x}_t) \approx -ts_{\phi_0}(\mathbf{x}_t, t), \tag{1}$$

where  $s_{\phi_0}(\mathbf{x}_t, t)$  is a neural approximation of  $\nabla \log p_t(\mathbf{x}_t)$ . Consequently, generating from DM is equivalent to solving the PF-ODE, starting from noise randomly sampled from the prior distribution.

Modern solvers of the PF-ODE [10, 17] have significantly accelerated sampling speed, reducing the required network evaluations from hundreds to tens. To further speed up sampling, diffusion model are distilled into few-step generators, allowing multiple denoising steps to be performed in a single network evaluation [18, 7, 8]. This involves training a student model to learn the noise-to-data PF-ODE trajectory of a pre-trained teacher model. Recent studies [19–21], such as Latent Consistency Models (LCM) [1], scale-up this distillation method to high-resolution generation by distilling diffusion models trained on latent space of a pre-trained AE. These models incur additional computational costs by having to decode the generated latent back into pixel space. For example, in distilled SD v1.5, while single-step latent generation takes 0.04 seconds per image, the decoder requires 0.05 seconds per image for this mapping (see Table 1).

When considering generation at higher resolutions, two main options exist. The first, Latent Diffusion Model (LDM) [12, 22], involves obtaining an AE for high-resolution images, followed by training a latent DM in AE’s latent space, and finally distilling the DM. This method is expensive as it requires repeating the entire training pipeline. Alternatively, Cascaded Diffusion Model (CDM) [6, 23] employs an upsampling approach, which upsamples generated data from a low-resolution DM or its distilled model to its higher resolution counterpart using an upsampler DM. However, training this upsampler DM incurs costs comparable to those of training high-dimensional DMs, making it an expensive procedure as well. Moreover, the feasibility of distillation methods on CDMs has not yet fully investigated in literature. These limitations highlight the need for a model that can be easily adapted to handle high resolutions without the need for expensive training.

### 3 Progressive Growing of Diffusion Autoencoder

This section establishes the foundation of PaGoDA, a model that alleviates the previously mentioned problems of distillation. PaGoDA adopts an AE structure. During training, PaGoDA’s generator can be adapted to resolution changes without the need for expensive retraining. In inference, PaGoDA doesn’t need to decode generated latents back to data, as it is directly trained on pixel space, thereby accelerating sampling compared to (distilled) latent diffusion models.

#### 3.1 Objective Function

PaGoDA employs a pre-trained DM at a low (base) resolution space  $\mathbb{R}^d$  to establish a fixed and deterministic encoder. At the base resolution, for each data point  $\mathbf{x} \in \mathbb{R}^d$  and a given condition (such as class or prompt)  $\mathbf{c}$ , the latent representation  $E(\mathbf{x}, \mathbf{c})$ , with  $E(\cdot, \mathbf{c}): \mathbb{R}^d \rightarrow \mathbb{R}^d$ , is obtained by solving the pre-trained DM’s PF-ODE of Eq. (1) forward in time, evolving from the clean base resolution data  $\mathbf{x}$  (time 0) to its noisy counterpart (time  $T$ ). PaGoDA’s generator  $G_\theta: \mathbb{R}^d \rightarrow \mathbb{R}^d$  is then trained using a reconstruction loss:

$$\mathcal{L}_{\text{rec}}(G_\theta) := \mathbb{E}_{p_{\text{data}}(\mathbf{x}, \mathbf{c})} \left[ \left\| \mathbf{x} - G_\theta(E(\mathbf{x}, \mathbf{c}), \mathbf{c}) \right\|_2^2 \right].$$

For conditional generation (with condition  $\mathbf{c}$ ), we draw a random noise  $\mathbf{z} \in \mathbb{R}^d$  from the Gaussian prior distribution and feed this noise to the trained one-step generator  $G_\theta(\mathbf{z}, \mathbf{c})$  to synthesize samples.

The key challenge in PaGoDA training lies in aligning the aggregated posterior, the distribution of latent  $E(\mathbf{x}, \mathbf{c})$  when  $\mathbf{x}, \mathbf{c} \sim p_{\text{data}}(\mathbf{x}, \mathbf{c})$ , with the prior distribution  $p_{\text{prior}}(\mathbf{z})$ . Although a well-trained DM’s PF-ODE ensures close alignment between its aggregated posterior and the prior distribution in population, the finite amount of available data restricts training to cover only a limited number of latents. Consequently, a significant portion of the prior distribution remains unseen during decoder training, leading to overfitting. As the PaGoDA encoder is not trainable, this prior hole cannot be filled with an auxiliary regularizer of the encoder, such as the KL term in Variational Autoencoder’s ELBO [4], resulting in high reconstruction quality but poor generation quality of PaGoDA.

Motivated from this, we propose to combine the reconstruction loss with the adversarial loss

$$\mathcal{L}_{\text{adv}}(G_\theta, D_\psi) := \mathbb{E}_{p_{\text{data}}(\mathbf{x}, \mathbf{c})} \left[ \log D_\psi(\mathbf{x}, \mathbf{c}) \right] + \mathbb{E}_{p_{\text{prior}}(\mathbf{z}) p_{\text{data}}(\mathbf{c})} \left[ \log \left( 1 - D_\psi(G_\theta(\mathbf{z}, \mathbf{c}), \mathbf{c}) \right) \right].$$

Here,  $D_\psi$  is a discriminator that classifies the real and fake samples by maximizing the adversarial loss, and  $p_{\text{data}}(\mathbf{c})$  is the marginal condition distribution of the dataset. The second term of  $\mathcal{L}_{\text{adv}}$ ,

Table 1: Model comparison.

Model	Sampling NFE	Sample Quality	Training Stability
VAE [4]	1	△	☹
GAN [5]	1	☹	△
DM [2]	Many	☹	☹
LCM [1]	1+1	☹	☹
PaGoDA	1	☹	☹

involving  $G_\theta(\mathbf{z}, \mathbf{c})$  with  $\mathbf{z}$  sampled from the prior, ensures that the decoder is exposed to the full support of the prior distribution during training. While PaGoDA incorporates the adversarial loss, the reconstruction loss encourages the decoder to encompass all training data. Therefore, the GAN loss accounts for underrepresented areas in the prior distribution without hurting sample diversity.

Overall, we train PaGoDA with the mini-max optimization of the following combined objective:

$$\min_{G_\theta} \max_{D_\psi} \mathcal{L}_{\text{PaGoDA}}(G_\theta, D_\psi) := \min_{G_\theta} \left[ \mathcal{L}_{\text{rec}}(G_\theta) + \lambda \max_{D_\psi} \mathcal{L}_{\text{adv}}(G_\theta, D_\psi) \right]. \quad (2)$$

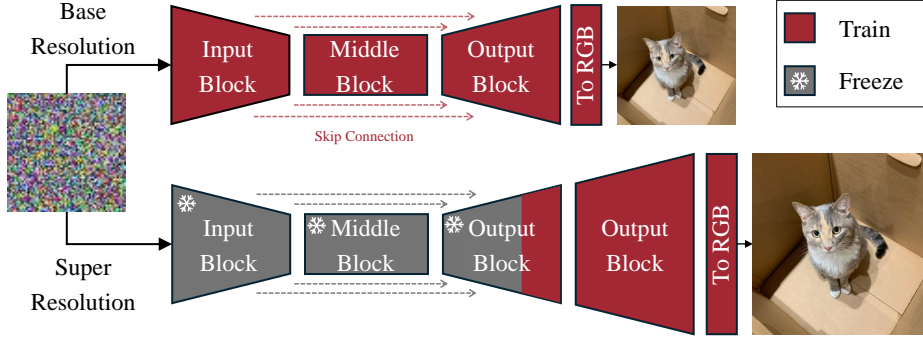


Figure 3: PaGoDA’s decoder architecture.

### 3.2 Progressively Growing Decoder for Higher Resolution

For higher resolution, we introduce PaGoDA’s encoding and progressive decoding process.

**PaGoDA’s Encoding.** The encoding process, as illustrated in Figure 2, is still fixed and begins with downsampling the high-resolution data  $\mathbf{x} \in \mathbb{R}^{2d}$  to the base resolution of the pre-trained DM, resulting in  $\mathbf{x}_{\text{base}} \in \mathbb{R}^d$ . As described in Section 3.1, the latent representation  $E(\mathbf{x}, \mathbf{c})$ , now with  $E(\cdot, \mathbf{c}): \mathbb{R}^{2d} \rightarrow \mathbb{R}^d$ , for  $\mathbf{x}$  and condition  $\mathbf{c}$  is obtained by solving the pre-trained DM’s PF-ODE forward in time, starting from the clean data  $\mathbf{x}_{\text{base}}$  to obtain its noisy counterpart.

**PaGoDA’s Decoding.** Figure 3 illustrates the progressively growing PaGoDA decoder  $G_\theta$ , now mapping from  $\mathbb{R}^d$  to  $\mathbb{R}^{2d}$ . We use a U-Net [24], initialized with the pre-trained DM, as PaGoDA’s base resolution decoder (mapping from  $\mathbb{R}^d$  to  $\mathbb{R}^d$ ) and train it with Eq. (2). Subsequently, as depicted in the bottom row of Figure 3, additional ResNet [25] blocks are appended after the output block of the base resolution’s U-Net. Within the base resolution’s U-Net, we freeze its input, middle, and output blocks except for the last few layers (previously highest resolution block) during super-resolution training, following the practice in PG GAN [9]. The unfrozen latter part of the network is then trained for super-resolution. This progressive growing process can be iterated to upsample the output until it reaches to the desired resolution ( $2^n d$  for some  $n \in \mathbb{N}$ ). This approach is not only cost-effective but also ensures stable training of the entire network. By partitioning the training process, we can maximize the batch size for each training stage, enhancing both semantic quality and fine-details within budget constraints.

### 3.3 Optimality Guarantee and Training Stability

Training PaGoDA’s generator solely with  $\mathcal{L}_{\text{rec}}$  restricts the quality of the decoder to that of the teacher diffusion. While refining the teacher model is a viable option for better one-step generation (see Appendix B.1 for details), Theorem 3.1 suggests that combining the GAN loss with the reconstruction loss provides another method to refine the one-step decoder. This integration ensures that the density produced by an optimal generator precisely matches the data distribution:

**Theorem 3.1.** *Let  $\lambda > 0$ . Suppose  $D^*(G) \in \arg \max_D \mathcal{L}_{\text{adv}}(G, D)$ . If both PaGoDA’s reconstruction loss and GAN loss share a common minimizer  $G^*$ , then  $p_{G^*}(\mathbf{x}|\mathbf{c}) = p_{\text{data}}(\mathbf{x}|\mathbf{c})$  for all condition  $\mathbf{c}$  sampled from  $p_{\text{data}}(\mathbf{c})$ . Here,  $p_{G^*}$  is the generative distribution learned by optimizing Eq. (2).*

Theorem 3.1 establishes that PaGoDA can function as a standalone *generative model*, effectively approximating the data distribution. Additionally, Theorem 3.2 shows that PaGoDA’s training is

stable at the base resolution with the help of reconstruction loss, even with adversarial training. It further reinforces PaGoDA as a *robust* generative model. We empirically observe that PaGoDA can be trained effectively without many of the techniques typically used to stabilize GANs [26, 27].

**Theorem 3.2.** [Informal] *Let  $E$  be a fixed deterministic encoder. Suppose that at the generator’s equilibria  $G^*$  of Eq. (2),  $p_{G^*}(\mathbf{x}|\mathbf{c}) = p_{\text{data}}(\mathbf{x}|\mathbf{c})$ , and  $\mathbf{x} = G^*(E(\mathbf{x}, \mathbf{c}), \mathbf{c})$  for  $\mathbf{x} \in \text{supp}(p_{\text{data}}(\cdot|\mathbf{c}))$  and  $\mathbf{c} \sim p_{\text{data}}(\mathbf{c})$ . Then, under conditions similar to those found in the stability literature for improving GAN [28, 27], training with Eq. (2) is stable (gradient descent locally converges to its equilibria).*

We refer to Theorems B.4 and B.9 for rigorous and extended versions of Theorems 3.1 and 3.2, respectively. All proofs can be found in Appendix B.

## 4 PaGoDA with Classifier-Free Guidance

This section proposes a methodology to incorporate CFG into PaGoDA for Text-to-Any generation (with the focus on T2I). CFG guides the denoising process by adjusting the conditional score gradient  $\nabla \log p_t(\mathbf{x}_t|\mathbf{c})$  into a guided score  $\nabla \log p_t(\mathbf{x}_t|\mathbf{c}) + (\omega - 1)\nabla \log p(\mathbf{c}|\mathbf{x}_t)$  [29, 16], resulting in the sample distribution (with oracle score), starting from the prior distribution  $p_{\text{prior}}(\mathbf{z})$ , to be

$$p_{\text{data}}(\mathbf{x}|\mathbf{c}, \omega) \propto p_{\text{data}}(\mathbf{x}|\mathbf{c})^\omega p_{\text{data}}(\mathbf{x})^{1-\omega}.$$

### 4.1 Classifier-Free GAN

The loss introduced in Section 3.1 only ensures the estimation of  $p_{\text{data}}(\mathbf{x}|\mathbf{c})$  with the decoder, not of  $p_{\text{data}}(\mathbf{x}|\mathbf{c}, \omega)$ . Notably, existing literature on GAN [30, 31, 21, 32] has not explored the use of CFG. Here, we introduce *classifier-free GAN* to integrate CFG into PaGoDA for better generation.

To illustrate the design of classifier-free GAN, we first consider the loss:

$$\mathcal{L}_{\text{adv}}^{\mathbf{c}, \omega}(G_\theta, D_\psi) := \mathbb{E}_{p_{\text{data}}(\mathbf{x}|\mathbf{c}, \omega)} \left[ \log D_\psi(\mathbf{x}, \mathbf{c}, \omega) \right] + \mathbb{E}_{p_{G_\theta}(\mathbf{x}|\mathbf{c}, \omega)} \left[ \log \left( 1 - D_\psi(\mathbf{x}, \mathbf{c}, \omega) \right) \right],$$

where now both generator and discriminator incorporates  $\omega$  as an additional condition [19]. From the standard GAN argument [5], this GAN loss guarantees the optimal generator to match to the data distribution, i.e.,  $p_{G^*}(\mathbf{x}|\mathbf{c}, \omega) = p_{\text{data}}(\mathbf{x}|\mathbf{c}, \omega)$ . However, as sampling from  $p_{\text{data}}(\mathbf{x}|\mathbf{c}, \omega)$  is infeasible in general, we use the Bayes formula

$$p_{\text{data}}(\mathbf{x}, \mathbf{c})p(\omega|\mathbf{x}, \mathbf{c}) = p_{\text{data}}(\mathbf{c})\pi(\omega)p_{\text{data}}(\mathbf{x}|\mathbf{c}, \omega),$$

where both representations are two different ways to decompose the joint distribution over  $(\mathbf{x}, \mathbf{c}, \omega)$  with  $\pi(\omega)$  being the prior distribution of the CFG scale,  $\omega$ , set to be a uniform distribution over  $[1, 10]$ . From the Bayes formula, if we have access to  $p(\omega|\mathbf{x}, \mathbf{c})$ , sampling  $(\mathbf{x}, \mathbf{c}, \omega)$  from  $p_{\text{data}}(\mathbf{c})\pi(\omega)p_{\text{data}}(\mathbf{x}|\mathbf{c}, \omega)$  is equivalent to sampling  $(\mathbf{x}, \mathbf{c})$  from  $p_{\text{data}}(\mathbf{x}, \mathbf{c})$  first from the real dataset and subsequently sample  $\omega \sim p(\omega|\mathbf{x}, \mathbf{c})$ . Hence, we introduce the classifier-free GAN loss with the following implementable reformulation:

$$\begin{aligned} \mathcal{L}_{\text{adv}}^{\text{CFG}}(G_\theta, D_\psi) &:= \mathbb{E}_{p_{\text{data}}(\mathbf{c})\pi(\omega)} \left[ \mathcal{L}_{\text{adv}}^{\mathbf{c}, \omega}(G_\theta, D_\psi) \right] \\ &= \mathbb{E}_{p_{\text{data}}(\mathbf{x}, \mathbf{c})p(\omega|\mathbf{x}, \mathbf{c})} \left[ \log D_\psi(\mathbf{x}, \mathbf{c}, \omega) \right] + \mathbb{E}_{p_{\text{data}}(\mathbf{c})\pi(\omega)p_{G_\theta}(\mathbf{x}|\mathbf{c}, \omega)} \left[ \log \left( 1 - D_\psi(\mathbf{x}, \mathbf{c}, \omega) \right) \right]. \end{aligned}$$

We approximate  $p(\omega|\mathbf{x}, \mathbf{c})$  with a U-Net encoder network with 1-dimensional output, called *CFG weight estimator*  $\omega_\phi$ . The input of  $\omega_\phi$  is a single-channel matrix with  $(i, j)$ -th value as the multiplication of the  $i/j$ -th values of  $\mathbf{x}/\mathbf{c}$  CLIP embeddings, respectively. As this matrix is high-dimensional, we input the downsampled  $64 \times 64 \times 1$  matrix to the U-Net encoder. These CLIP embeddings are also used to condition the network. With a pre-trained diffusion model sufficiently close to the data distribution, we train the CFG weight estimator by minimizing  $\mathbb{E}_{p_{\text{prior}}(\mathbf{z})p_{\text{data}}(\mathbf{c})\pi(\omega)} [\|\omega - \omega_\phi(\hat{\mathbf{x}}(\mathbf{z}, \mathbf{c}, \omega), \mathbf{c})\|_2^2]$ , where  $\hat{\mathbf{x}}(\mathbf{z}, \mathbf{c}, \omega)$  is a clean base-resolution sample drawn the teacher diffusion. Then,  $\omega_\phi(\mathbf{x}, \mathbf{c})$ -value becomes the point estimation of  $p(\omega|\mathbf{x}, \mathbf{c})$ . For higher resolution PaGoDA training, we downsample  $\mathbf{x}$  to  $\mathbf{x}_{\text{base}}$  and put this to the CFG weight estimator to approximate the most likely  $\omega$ .

### 4.2 Objective Function with Classifier-Free Guidance

Table 2: Experimental results of PaGoDA on ImageNet.

Model	Sampling NFE	Without CFG			With CFG			Without CFG			With CFG		
		FID ↓	IS ↑	Recall ↑	FID	IS	Recall	FID	IS	Recall	FID	IS	Recall
<b>64<sup>2</sup> resolution</b>													
RIN [34]	250	1.23	66.5	-	-	-	-	2.75	144.1	-	-	-	-
simple Diffusion [35]	250	-	-	-	-	-	-	1.91	171.9	-	2.05	189.9	-
VDM++ [36]	79	1.43	63.7	-	-	-	-	1.75	171.1	-	1.78	190.5	-
StyleGAN-XL [37]	1	-	-	-	1.51	<b>82.35</b>	0.52	-	-	-	1.81	<b>200.55</b>	0.55
CTM [8]	1	1.92	70.38	0.57	-	-	-	-	-	-	-	-	-
PaGoDA (ours)	1	<b>1.21</b>	76.47	<b>0.63</b>	-	-	-	<b>1.48</b>	174.36	<b>0.61</b>	-	-	-
<b>128<sup>2</sup> resolution</b>													
<b>256<sup>2</sup> resolution</b>													
DiT-XL [38]	250	9.62	121.5	-	2.27	278.2	-	12.03	105.3	-	3.04	240.8	-
simple Diffusion [35]	250	2.77	211.8	-	2.44	256.3	-	3.54	205.3	-	3.02	248.7	-
VDM++ [36]	250	2.40	225.3	-	2.12	267.7	-	2.99	232.2	-	2.65	278.1	-
EDM2-XXL [39]	63	-	-	-	-	-	-	1.91	-	-	1.81	-	-
StyleGAN-XL [37]	1	-	-	-	2.30	<b>265.12</b>	0.53	-	-	-	2.41	<b>267.75</b>	0.52
PaGoDA (ours)	1	<b>1.56</b>	259.61	<b>0.59</b>	-	-	-	<b>1.80</b>	251.31	<b>0.58</b>	-	-	-
<b>512<sup>2</sup> resolution</b>													

For the reconstruction loss, we define  $E(\mathbf{x}, \mathbf{c}, \omega)$  as the latent obtained with the  $\omega$ -guided PF-ODE. Then, the latent distribution of  $E$  over the data distribution  $p_{\text{data}}(\mathbf{x}, \mathbf{c})$  no longer aligns with the prior distribution empirically. Figure 4 visualizes the output latent from an image, varying the CFG scales. As  $\omega$  increases, the latent gradually deviates from a random noise, and pertains more signal from the original image.

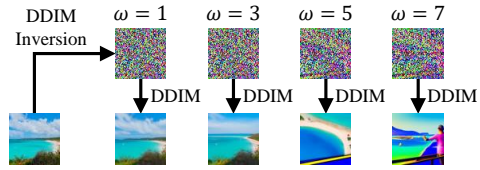


Figure 4: The latent from DDIM inversion with large CFG attains significant amount of original signal, leading poor latent quality.

Therefore, we maintain the original reconstruction loss (i.e.,  $\omega = 1$ ), while supplementing it with the distillation loss  $\mathcal{L}_{\text{dstl}}^{\text{CFG}}(G_{\theta}) = \mathbb{E}_{p_{\text{prior}}(\mathbf{z})p_{\text{data}}(\mathbf{c})\pi(\omega)}[\|\hat{\mathbf{x}}(\mathbf{z}, \mathbf{c}, \omega) - G_{\theta}(\mathbf{z}, \mathbf{c}, \omega)\|_2^2]$  to regularize the decoder when  $\omega > 1$ . Additionally, we can also leverage CLIP similarity [33] as a regularizer to further improve the text-sample alignment. In summary, we train PaGoDA with

$$\mathcal{L}_{\text{PaGoDA}}^{\text{CFG}}(G_{\theta}, D_{\psi}) := \mathcal{L}_{\text{rec}} + \mathcal{L}_{\text{dstl}}^{\text{CFG}} + \lambda \mathcal{L}_{\text{adv}}^{\text{CFG}} + \mathcal{L}_{\text{CLIP}}, \quad (3)$$

where  $\mathcal{L}_{\text{CLIP}}(G_{\theta}) := -\frac{1}{2} \mathbb{E}_{p_{\text{prior}}(\mathbf{z})p_{\text{data}}(\mathbf{c})\pi(\omega)}[\text{CLIP}(G_{\theta}(\mathbf{z}, \mathbf{c}, \omega), \mathbf{c})]$  is the CLIP similarity [30, 31], the dot product of image/text embeddings from pre-trained ViT-L/14 [33].

For super-resolution training, it is infeasible to directly use  $\mathcal{L}_{\text{dstl}}^{\text{CFG}}$  at higher resolution because  $\hat{\mathbf{x}}$  generated from a pre-trained DM is of base resolution. However, we can still train our decoder with the distillation loss by comparing the downsampled output image and the teacher diffusion’s image  $\hat{\mathbf{x}}$  at the base resolution, thereby enhancing training stability, particularly at the large CFG scales. Consequently, we still employ the loss of Eq. (3) for our super-resolution training.

## 5 Experiments

### 5.1 Class-Conditional ImageNet Generation

We conduct experiments on ImageNet using PaGoDA without CFG to validate the core algorithm described in Section 3. For the experiment, we utilize the diffusion scheduling suggested by EDM [40]. Before training, we collect latent representations  $\mathbf{z}$  for all ImageNet data  $(\mathbf{x}, \mathbf{c})$  using the Heun method [40] with 40 timesteps (79 NFE) to solve EDM’s PF-ODE from time 0 to  $T$ . Throughout the experiments, we maintain the batch size to be 256 for both  $\mathcal{L}_{\text{rec}}$  and  $\mathcal{L}_{\text{adv}}$  in PaGoDA loss of Eq. (2).

We initialize our base resolution generator with the pre-trained diffusion U-Net. Following CTM [8], we implement adaptive weighting [41] with  $\lambda = 0.2 \frac{\|\nabla_{\theta^l} \mathcal{L}_{\text{rec}}\|_2^2}{\|\nabla_{\theta^l} \mathcal{L}_{\text{adv}}\|_2^2}$ , where  $\theta^l$  represents the last layer of the generator. Without this, GAN dominates the training if weight is larger than 2.

For higher resolution generation, we double the previous resolution by adding two auxiliary ResNet blocks followed by one upsampler ResNet block. The previously trained generator remains frozen except for the highest resolution blocks, which are unfrozen. We then train the newly added blocks along with these unfrozen parts, using a fixed GAN weight of  $\lambda = 1.0$ . Appendix A.1 provides

Table 3: Ablation of base resolution.

Model	Resolution	NFE	FID	Resolution	NFE	FID	Speed [s]	Params
Pixel Teacher Diffusion	$32^2$	79	1.75	$64^2$	79	2.44	3.16s	296M
PaGoDA	$32^2 \rightarrow 32^2$	1	0.79	$64^2 \rightarrow 64^2$	1	1.21	0.040s	296M
	$32^2 \rightarrow 64^2$	1	1.34	$64^2 \rightarrow 128^2$	1	1.48	0.041s	299M
	$32^2 \rightarrow 128^2$	1	1.61	$64^2 \rightarrow 256^2$	1	1.56	0.044s	301M
	$32^2 \rightarrow 256^2$	1	1.83	$64^2 \rightarrow 512^2$	1	1.80	0.046s	302M

Table 4: Comparison on upsampling.

Model	Resolution	Params	NFE	FID
EDM2	$64^2$ DM	1.1B	63	1.33
	$512^2$ LDM	1.1B	63+1	1.96
PaGoDA	$64^2$ DM (teacher)	0.3B	79	2.44
	$64^2 \rightarrow 64^2$	0.3B	1	1.21
	$64^2 \rightarrow 512^2$	0.3B	1	1.80

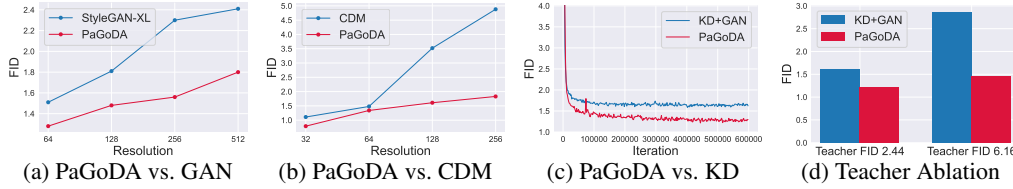


Figure 5: Experimental results of PaGoDA on ImageNet with various scenarios.



Figure 6: Upsampling comparison of PaGoDA and StyleGAN-XL.

additional details. By freezing part of the trained generator, we achieve greater stability in super-resolution training without the need for adaptive weighting.

Table 2 presents the performance of PaGoDA. Our model consistently outperforms all existing models across all resolutions, achieving these SOTA FIDs without the need of CFG and any other stabilization tricks for GAN. Remarkably, PaGoDA’s Inception Score (IS) [42] is on par with other diffusion and GAN models that employed classifier-free guidance, which implies that PaGoDA samples are as distinctive as CFG samples. Also, PaGoDA generates samples as diverse as the real data distribution, evidenced by diversity recall metric [43], where the PaGoDA reports 0.63 for  $64^2$  resolution (data’s recall is 0.67). In contrast, StyleGAN-XL is far behind of PaGoDA in terms of the diversity metric, reporting 0.52 for  $64^2$  resolution. Note that we used StyleGAN-XL’s discriminator in PaGoDA training, implying that the reconstruction loss significantly improves the sample diversity.

## 5.2 Controlled Model Analysis

**Base Resolution Ablation.** Table 3 evaluates PaGoDA, starting with two different base resolutions,  $32^2$  and  $64^2$ . For the  $32^2$  teacher diffusion, we utilize the EDM [40] with a batch size of 4096. For the  $64^2$  model, we use a pre-trained DM from CM [7]. Table 3 indicates that both  $32^2$  and  $64^2$  serve as effective base resolutions, though performance decreases with higher compression rates.

**Inference Overhead by Resolution.** Table 3 details how changes in resolution affect the sampling speed and parameter counts. According to experimental results, our progressively growing decoder manages to perform upsampling with only a minimal increase in parameter numbers. Consequently, the sampling speed (measured on NVIDIA H100) remains largely unaffected by resolution changes.

**Comparison to SD in Upsampling.** Table 4 provides a comparative analysis of the upsampling capabilities of PaGoDA and SD, with EDM2-XL [39] serving as the backbone architecture for SD. In its experiments, EDM2 first trained a pixel diffusion in a  $64 \times 64 \times 3$  pixel space, and then EDM2 trained the same model in a  $64 \times 64 \times 4$  latent space; the only change was an increase in the input channel to 4. The difference in FIDs between  $64$  (FID 1.33) and  $512$  (FID 1.96) resolutions within EDM2 highlights the upsampling effectiveness of SD. Similarly, for PaGoDA, the disparity in FIDs between these resolutions underlines its upsampling power. In comparison to SD, PaGoDA demonstrates a slight edge in upsampling capabilities. Furthermore, our results are particularly encouraging, showcasing superior performance even with an underperforming smaller teacher model.

**Comparison to GAN in Upsampling.** Figure 5-(a) compares PaGoDA with StyleGAN-XL, adopting its discriminator architecture for PaGoDA training. Unlike StyleGAN-XL, which often fails when

Table 5: Experimental results on T2I. FID-30K is based on MSCOCO-2014 [45] validation data. Speed is measured on A100.

Model	Params	Speed [s]	FID ↓
eDiff-I [46]	9.1B	32.0s	6.95
LDM [12]	1.5B	9.4s	12.63
Imagen [23]	3.0B	9.1s	7.27
SD1.5 [12]	0.9B	2.9s	9.62
PixArt- $\alpha$ [47]	0.6B	-	10.65
Scott [48]	0.9B	0.13s	12.22
GigaGAN [30]	1.0B	0.13s	9.09
StyleGAN-T [31]	1.0B	0.10s	13.90
InstaFlow [20]	0.9B	0.09s	13.10
UFOGen [49]	0.9B	0.09s	12.78
DMD [50]	0.9B	0.09s	11.49
LAFITE [51]	75M	0.02s	26.94
PaGoDA (ours)	0.9B	0.05s	10.23

Table 6: Experimental results on T2I. FID-5K is measured on MSCOCO-2017 [45] validation data. CLIP score is measured by the ViT-g/14 backbone. Our model uses DeepFloyd-IF as the pre-trained diffusion.

Model	Params	NFE	Speed [s]	FID ↓	CLIP ↑
SD1.5 [12]	0.9B	50+1	2.59s	19.1	31.3
DeepFloyd-IF [52]	0.9B	27	2.95s	22.3	28.1
<b>Latent Distillation Models based on SD1.5 [12]</b>					
CAD [19]	0.9B	8+1	0.34s	24.2	30.0
PD [6]	0.9B	4+1	0.21s	26.4	30.0
LCM [1]	0.9B	2+1	0.13s	30.4	29.3
InstaFlow [20]	0.9B	1+1	0.09s	23.4	30.4
UFOGen [49]	0.9B	1+1	0.09s	22.5	31.1
Scott [48]	0.9B	1+1	0.09s	21.9	31.2
ADD [21]	0.9B	1+1	0.09s	19.7	32.6
<b>Pixel Distillation Model based on DeepFloyd-IF [52]</b>					
PaGoDA (ours)	0.9B	1	0.05s	20.4	31.2

trained from scratch, PaGoDA exhibits training stability across various GAN weight hyperparameters and does not require conventional GAN stabilizing techniques. Not only outperforming StyleGAN-XL in both diversity and quality, PaGoDA further excels in upsampling, maintaining sample location consistency across resolutions as shown in Figure 6. This consistency allows for controllable generation at low resolutions, followed by the generation of high-resolution outputs based on the controlled latent. In contrast, StyleGAN-XL lacks this capability for efficient latent manipulation as its sample location varies with resolution, preventing a seamless transition from low to high-resolution control.

**Comparison to CDM in Upsampling.** Figure 5-(b) compares PaGoDA with Cascaded Diffusion Models (CDM) [44], an upsampling method in pixel DMs. Unlike PaGoDA’s consistent FID curve, CDM’s FID curve deteriorates significantly beyond the  $128^2$  resolution, mirroring the performance curve typical of DMs. This decline is attributed to CDM’s approach of training a upsampling DM, using a low-resolution image as the conditioning input. While this allows CDM the flexibility to independently manage each upsampling event, it inherently slows down the process due to the requisite independent denoising at every upsampling. In contrast, PaGoDA achieves high-resolution output via a single evaluation, considerably accelerating the sampling speed relative to CDM.

**Comparison to KD in Base Resolution.** Figure 5-(c) compares PaGoDA with a distillation method (noise-to-data), called Knowledge Distillation (KD) [18]. We utilize the same pre-trained teacher model. However, in KD+GAN, the training data pair  $(\mathbf{x}, \mathbf{z})$  is formed by solving PF-ODE in reverse time, starting from  $\mathbf{z} \sim p_{\text{prior}}(\mathbf{z})$ , contrasting with PaGoDA’s construction by solving PF-ODE in forward time, starting from  $\mathbf{x} \sim p_{\text{data}}(\mathbf{x})$ . The discrepancy in training data construction influences the models’ convergence, highlighted by PaGoDA’s better FIDs. This experimental observation aligns with our theoretical expectations: PaGoDA’s optimal generator, demonstrated in Theorem 3.1, learns the true data distribution, yielding superior FID scores. In contrast, KD+GAN’s generator may compromise between the data and teacher’s distributions, potentially leading to suboptimal results.

**Comparison to KD in Teacher.** Figure 5-(d) compares how the performance of PaGoDA and KD is influenced by the teacher model. Using Heun’s solver, we generate two different teacher trajectories for distillation, with NFEs 79 and 15, resulting in teacher FIDs of 2.44 and 6.16, respectively. PaGoDA and KD+GAN are tested under identical experimental conditions, differing only in their data collection methods (KD’s noise-to-data versus PaGoDA’s data-to-noise). The performance gap observed may stem from KD directly distilling underperforming samples from the teacher, while PaGoDA reconstructs real data despite potential errors in the latents. These results also support Theorem 3.1, indicating that the optimal PaGoDA generator recovers the data distribution.

### 5.3 Text-to-Image Generation

We collect the latents of the CC12M dataset [53] through DDIM inversion for  $\omega = 1$  with 100 DDIM steps. For GAN training dataset, we utilize the filtered COYO-700M [54] dataset, where only data with CLIP score (measured by ViT-B/32 [55]) higher than 32, and aesthetic score-v2 [56] higher than 5.0. We use the DeepFloyd-IF model [52], trained on  $64^2$  pixel space, as our teacher diffusion. For CFG samples, we apply DDIM with 27 steps with text prompts from COYO-700M dataset to construct the dataset for the distillation  $\mathcal{L}_{\text{dst}}^{\text{cfg}}$  loss, see Appendix A.2 for experimental details.



Table 5 compares our model against existing T2I benchmarks. Among models that generate samples within 0.1 seconds, ours exhibits the highest performance. Notably, LAFITE [51] produces samples in just 0.02 seconds using fewer parameters, but at the cost of significantly lower sample quality. In contrast, our speed strikes a balance between LAFITE [51] and distilled SD, offering superior sample quality compared to its baselines. Further examples of our model’s outputs are showcased in Figure 1.

Table 6 presents the outcomes of experiments conducted in controlled settings. For a balanced evaluation, we compare our PaGoDA with latent distillation models derived from SD v1.5 [12], as both teacher models, DeepFloyd-IF and SD1.5, exhibits similar performances. The findings shown in Table 6 reveal that our model is competitive with leading distillation models. We could further improve the CLIP performance by increasing  $\mathcal{L}_{\text{CLIP}}$  scale, achieving to 32.8 CLIP value without a significant loss in FID. However, as CLIP does not yield substantially meaningful differences beyond a certain level in text-image alignment, we opt to report the model’s performance with the best FID setup. In summary, our model delivers performance almost identical to that of distilled SD1.5 or teacher DeepFloyd, yet operates approximately twice as fast with comparable number of parameters.

Table 7 presents the ablation study of the objective function on  $64^2$  base resolution. We compare diverse loss variations, including the original PaGoDA loss,  $\mathcal{L}_{\text{rec}} + \mathcal{L}_{\text{adv}}$  without CFG, and the loss  $\mathcal{L}_{\text{dstl}}^{\text{CFG}} + \mathcal{L}_{\text{adv}}^{\text{CFG}}$  without reconstruction loss. The vanilla PaGoDA loss can only distill  $\omega = 1$ , and the performance is behind of the other models. Using previous guided distillation loss combined with adversarial loss, we achieves better performance than the vanilla PaGoDA loss. On top of that, if we guide the decoder with the real data using the reconstruction loss, we observe additional performance gain. Using CLIP regularization further improves the performance, as discussed in Section 4.2.

Table 7: Ablation study on 64x64 generation.

Loss	FID ↓	CLIP ↑
$\mathcal{L}_{\text{rec}} + \mathcal{L}_{\text{adv}}$	31.1	26.4
$\mathcal{L}_{\text{dstl}}^{\text{CFG}} + \mathcal{L}_{\text{adv}}^{\text{CFG}}$	25.4	26.9
$\mathcal{L}_{\text{rec}} + \mathcal{L}_{\text{dstl}}^{\text{CFG}} + \mathcal{L}_{\text{adv}}^{\text{CFG}}$	22.6	27.6
PaGoDA ( $\mathcal{L}_{\text{PaGoDA}}^{\text{CFG}}$ )	<b>19.9</b>	<b>30.9</b>

#### 5.4 Applications: Controllable Generation and Inverse Problems

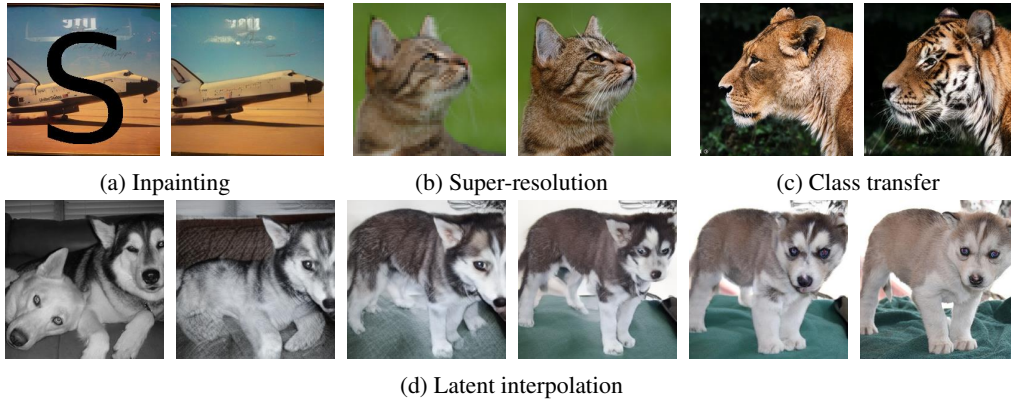


Figure 7: Controllable generation of PaGoDA with various tasks.

Once we have a trained PaGoDA decoder  $G_{\theta_0}$ , we can utilize it for solving inverse problems [57] and for controllable generation [58] in a training-free manner [59].

**Latent Optimization** We consider the inverse problem:  $\mathbf{y} = \mathcal{A}(\mathbf{x}) + \eta$ , where  $\mathbf{y}$  represents the observation, and  $\mathcal{A} : \mathbb{R}^d \rightarrow \mathbb{R}^m$  with  $d \geq m$  is a known operator. The restored data  $\mathbf{x}$  can be reconstructed by optimizing the latent. Specifically, if  $\mathbf{z}^* \in \arg \min_{\mathbf{z}} \|\mathbf{y} - \mathcal{A}(G_{\theta_0}(\mathbf{z}, \mathbf{c}))\|_2^2$ , then  $G_{\theta_0}(\mathbf{z}^*, \mathbf{c})$  is the best possible estimate of the solution for the inverse problem. Figure 7-(a) displays the outcomes of an inpainting task where latent optimization is employed with Adam optimizer [60].

**DDIM Inversion** Specific tasks, such as super-resolution illustrated in Figure 7-(b) and class transfer depicted in Figure 7-(c), can be effectively addressed without relying on latent optimization. For these tasks, we apply DDIM inversion to the downsampled observations, then map the DDIM latent back to RGB pixel by feeding the latent into the decoder. Generally, using DDIM inversion yields superior outcomes compared to latent optimization for these types of tasks.

**Latent Interpolation** Building on techniques from GAN research, we also explored latent interpolation for style mixing. Despite our model’s latent dimension being larger than the typical 512-dimensional style vector used in GAN, our observations indicate that latent mixing by slerp operation [61, 26] achieves effective results, as demonstrated in Figure 7-(d).

## 6 Conclusion

PaGoDA addresses the limitations of distillation-based DMs, where resolution is constrained by the teacher model. It efficiently encodes data into latent representations through downsampling and solves the teacher model’s probability flow ODE in a data-to-noise manner. The progressive expansion of the decoder provides a low-cost super-resolution generative model with inference speed faster than Stable Diffusion.

## References

- [1] Simian Luo, Yiqin Tan, Longbo Huang, Jian Li, and Hang Zhao. Latent consistency models: Synthesizing high-resolution images with few-step inference. *arXiv preprint arXiv:2310.04378*, 2023.
- [2] Jonathan Ho, Ajay Jain, and Pieter Abbeel. Denoising diffusion probabilistic models. *Advances in Neural Information Processing Systems*, 33:6840–6851, 2020.
- [3] Yang Song, Jascha Sohl-Dickstein, Diederik P Kingma, Abhishek Kumar, Stefano Ermon, and Ben Poole. Score-based generative modeling through stochastic differential equations. In *International Conference on Learning Representations*, 2020.
- [4] Diederik P Kingma and Max Welling. Auto-encoding variational bayes. *arXiv preprint arXiv:1312.6114*, 2013.
- [5] Ian Goodfellow, Jean Pouget-Abadie, Mehdi Mirza, Bing Xu, David Warde-Farley, Sherjil Ozair, Aaron Courville, and Yoshua Bengio. Generative adversarial nets. *Advances in neural information processing systems*, 27, 2014.
- [6] Tim Salimans and Jonathan Ho. Progressive distillation for fast sampling of diffusion models. In *International Conference on Learning Representations*, 2021.
- [7] Yang Song, Prafulla Dhariwal, Mark Chen, and Ilya Sutskever. Consistency models. *arXiv preprint arXiv:2303.01469*, 2023.
- [8] Dongjun Kim, Chieh-Hsin Lai, Wei-Hsiang Liao, Naoki Murata, Yuhta Takida, Toshimitsu Uesaka, Yutong He, Yuki Mitsufuji, and Stefano Ermon. Consistency trajectory models: Learning probability flow ode trajectory of diffusion. In *International Conference on Learning Representations*, 2024.
- [9] Tero Karras, Timo Aila, Samuli Laine, and Jaakko Lehtinen. Progressive growing of gans for improved quality, stability, and variation. *arXiv preprint arXiv:1710.10196*, 2017.
- [10] Jiaming Song, Chenlin Meng, and Stefano Ermon. Denoising diffusion implicit models. In *International Conference on Learning Representations*, 2020.
- [11] Xuan Su, Jiaming Song, Chenlin Meng, and Stefano Ermon. Dual diffusion implicit bridges for image-to-image translation. *arXiv preprint arXiv:2203.08382*, 2022.
- [12] Robin Rombach, Andreas Blattmann, Dominik Lorenz, Patrick Esser, and Björn Ommer. High-resolution image synthesis with latent diffusion models. In *Proceedings of the IEEE/CVF conference on computer vision and pattern recognition*, pages 10684–10695, 2022.
- [13] Haoye Lu, Yiwei Lu, Dihong Jiang, Spencer Ryan Szabados, Sun Sun, and Yaoliang Yu. Cm-gan: Stabilizing gan training with consistency models. In *ICML 2023 Workshop on Structured Probabilistic Inference & Generative Modeling*, 2023.
- [14] Martin Heusel, Hubert Ramsauer, Thomas Unterthiner, Bernhard Nessler, and Sepp Hochreiter. Gans trained by a two time-scale update rule converge to a local nash equilibrium. *Advances in neural information processing systems*, 30, 2017.
- [15] Olga Russakovsky, Jia Deng, Hao Su, Jonathan Krause, Sanjeev Satheesh, Sean Ma, Zhiheng Huang, Andrej Karpathy, Aditya Khosla, Michael Bernstein, et al. Imagenet large scale visual recognition challenge. *International journal of computer vision*, 115:211–252, 2015.
- [16] Jonathan Ho and Tim Salimans. Classifier-free diffusion guidance. In *NeurIPS 2021 Workshop on Deep Generative Models and Downstream Applications*, 2021.
- [17] Cheng Lu, Yuhao Zhou, Fan Bao, Jianfei Chen, Chongxuan Li, and Jun Zhu. Dpm-solver: A fast ode solver for diffusion probabilistic model sampling in around 10 steps. *Advances in Neural Information Processing Systems*, 35:5775–5787, 2022.
- [18] Eric Luhman and Troy Luhman. Knowledge distillation in iterative generative models for improved sampling speed. *arXiv preprint arXiv:2101.02388*, 2021.

- [19] Chenlin Meng, Robin Rombach, Ruiqi Gao, Diederik Kingma, Stefano Ermon, Jonathan Ho, and Tim Salimans. On distillation of guided diffusion models. In *Proceedings of the IEEE/CVF Conference on Computer Vision and Pattern Recognition*, pages 14297–14306, 2023.
- [20] Xingchao Liu, Xiwen Zhang, Jianzhu Ma, Jian Peng, et al. Instaflo: One step is enough for high-quality diffusion-based text-to-image generation. In *The Twelfth International Conference on Learning Representations*, 2023.
- [21] Axel Sauer, Dominik Lorenz, Andreas Blattmann, and Robin Rombach. Adversarial diffusion distillation. *arXiv preprint arXiv:2311.17042*, 2023.
- [22] Pablo Pernias, Dominic Rampas, Mats Leon Richter, Christopher Pal, and Marc Aubreville. Würstchen: An efficient architecture for large-scale text-to-image diffusion models. In *The Twelfth International Conference on Learning Representations*, 2023.
- [23] Chitwan Saharia, William Chan, Saurabh Saxena, Lala Li, Jay Whang, Emily L Denton, Kamyar Ghasemipour, Raphael Gontijo Lopes, Burcu Karagol Ayan, Tim Salimans, et al. Photorealistic text-to-image diffusion models with deep language understanding. *Advances in Neural Information Processing Systems*, 35:36479–36494, 2022.
- [24] Olaf Ronneberger, Philipp Fischer, and Thomas Brox. U-net: Convolutional networks for biomedical image segmentation. In *Medical image computing and computer-assisted intervention—MICCAI 2015: 18th international conference, Munich, Germany, October 5-9, 2015, proceedings, part III 18*, pages 234–241. Springer, 2015.
- [25] Sergey Zagoruyko and Nikos Komodakis. Wide residual networks. *arXiv preprint arXiv:1605.07146*, 2016.
- [26] Tero Karras, Samuli Laine, and Timo Aila. A style-based generator architecture for generative adversarial networks. In *Proceedings of the IEEE/CVF conference on computer vision and pattern recognition*, pages 4401–4410, 2019.
- [27] Lars Mescheder, Andreas Geiger, and Sebastian Nowozin. Which training methods for gans do actually converge? In *International conference on machine learning*, pages 3481–3490. PMLR, 2018.
- [28] Vaishnavh Nagarajan and J Zico Kolter. Gradient descent gan optimization is locally stable. *Advances in neural information processing systems*, 30, 2017.
- [29] Prafulla Dhariwal and Alexander Nichol. Diffusion models beat gans on image synthesis. *Advances in Neural Information Processing Systems*, 34:8780–8794, 2021.
- [30] Minguk Kang, Jun-Yan Zhu, Richard Zhang, Jaesik Park, Eli Shechtman, Sylvain Paris, and Taesung Park. Scaling up gans for text-to-image synthesis. In *Proceedings of the IEEE/CVF Conference on Computer Vision and Pattern Recognition*, pages 10124–10134, 2023.
- [31] Axel Sauer, Tero Karras, Samuli Laine, Andreas Geiger, and Timo Aila. Stylegan-t: Unlocking the power of gans for fast large-scale text-to-image synthesis. In *International conference on machine learning*, pages 30105–30118. PMLR, 2023.
- [32] Axel Sauer, Frederic Boesel, Tim Dockhorn, Andreas Blattmann, Patrick Esser, and Robin Rombach. Fast high-resolution image synthesis with latent adversarial diffusion distillation. *arXiv preprint arXiv:2403.12015*, 2024.
- [33] Alec Radford, Jong Wook Kim, Chris Hallacy, Aditya Ramesh, Gabriel Goh, Sandhini Agarwal, Girish Sastry, Amanda Askell, Pamela Mishkin, Jack Clark, et al. Learning transferable visual models from natural language supervision. In *International conference on machine learning*, pages 8748–8763. PMLR, 2021.
- [34] Allan Jabri, David Fleet, and Ting Chen. Scalable adaptive computation for iterative generation. *arXiv preprint arXiv:2212.11972*, 2022.
- [35] Emiel Hoogeboom, Jonathan Heek, and Tim Salimans. simple diffusion: End-to-end diffusion for high resolution images. In *International Conference on Machine Learning*, pages 13213–13232. PMLR, 2023.

- [36] Diederik P Kingma and Ruiqi Gao. Understanding diffusion objectives as the elbo with simple data augmentation. In *Thirty-seventh Conference on Neural Information Processing Systems*, 2023.
- [37] Axel Sauer, Katja Schwarz, and Andreas Geiger. Stylegan-xl: Scaling stylegan to large diverse datasets. In *ACM SIGGRAPH 2022 conference proceedings*, pages 1–10, 2022.
- [38] William Peebles and Saining Xie. Scalable diffusion models with transformers. In *Proceedings of the IEEE/CVF International Conference on Computer Vision*, pages 4195–4205, 2023.
- [39] Tero Karras, Miika Aittala, Jaakko Lehtinen, Janne Hellsten, Timo Aila, and Samuli Laine. Analyzing and improving the training dynamics of diffusion models. *arXiv preprint arXiv:2312.02696*, 2023.
- [40] Tero Karras, Miika Aittala, Timo Aila, and Samuli Laine. Elucidating the design space of diffusion-based generative models. *Advances in Neural Information Processing Systems*, 35:26565–26577, 2022.
- [41] Patrick Esser, Robin Rombach, and Bjorn Ommer. Taming transformers for high-resolution image synthesis. In *Proceedings of the IEEE/CVF conference on computer vision and pattern recognition*, pages 12873–12883, 2021.
- [42] Tim Salimans, Ian Goodfellow, Wojciech Zaremba, Vicki Cheung, Alec Radford, and Xi Chen. Improved techniques for training gans. *Advances in neural information processing systems*, 29, 2016.
- [43] Tuomas Kynkäänniemi, Tero Karras, Samuli Laine, Jaakko Lehtinen, and Timo Aila. Improved precision and recall metric for assessing generative models. *Advances in neural information processing systems*, 32, 2019.
- [44] Jonathan Ho, Chitwan Saharia, William Chan, David J Fleet, Mohammad Norouzi, and Tim Salimans. Cascaded diffusion models for high fidelity image generation. *The Journal of Machine Learning Research*, 23(1):2249–2281, 2022.
- [45] Tsung-Yi Lin, Michael Maire, Serge Belongie, James Hays, Pietro Perona, Deva Ramanan, Piotr Dollár, and C Lawrence Zitnick. Microsoft coco: Common objects in context. In *Computer Vision—ECCV 2014: 13th European Conference, Zurich, Switzerland, September 6–12, 2014, Proceedings, Part V 13*, pages 740–755. Springer, 2014.
- [46] Yogesh Balaji, Seungjun Nah, Xun Huang, Arash Vahdat, Jiaming Song, Qinsheng Zhang, Karsten Kreis, Miika Aittala, Timo Aila, Samuli Laine, et al. ediff-i: Text-to-image diffusion models with an ensemble of expert denoisers. *arXiv preprint arXiv:2211.01324*, 2022.
- [47] Junsong Chen, Jincheng Yu, Chongjian Ge, Lewei Yao, Enze Xie, Yue Wu, Zhongdao Wang, James Kwok, Ping Luo, Huchuan Lu, et al. Pixart- $\alpha$ : Fast training of diffusion transformer for photorealistic text-to-image synthesis. *arXiv preprint arXiv:2310.00426*, 2023.
- [48] Hongjian Liu, Qingsong Xie, Zhijie Deng, Chen Chen, Shixiang Tang, Fueyang Fu, Zhengjun Zha, and Haonan Lu. Scott: Accelerating diffusion models with stochastic consistency distillation. *arXiv preprint arXiv:2403.01505*, 2024.
- [49] Yanwu Xu, Yang Zhao, Zhisheng Xiao, and Tingbo Hou. Ufogen: You forward once large scale text-to-image generation via diffusion gans. *arXiv preprint arXiv:2311.09257*, 2023.
- [50] Tianwei Yin, Michaël Gharbi, Richard Zhang, Eli Shechtman, Fredo Durand, William T Freeman, and Taesung Park. One-step diffusion with distribution matching distillation. *arXiv preprint arXiv:2311.18828*, 2023.
- [51] Yufan Zhou, Ruiyi Zhang, Changyou Chen, Chunyuan Li, Chris Tensmeyer, Tong Yu, Jiuxiang Gu, Jinhui Xu, and Tong Sun. Towards language-free training for text-to-image generation. In *Proceedings of the IEEE/CVF Conference on Computer Vision and Pattern Recognition*, pages 17907–17917, 2022.

- [52] DeepFloyd Lab. If by deepfloyd lab at stabilityai. <https://github.com/deep-floyd/IF>, 2023.
- [53] Soravit Changpinyo, Piyush Sharma, Nan Ding, and Radu Soricut. Conceptual 12M: Pushing web-scale image-text pre-training to recognize long-tail visual concepts. In *CVPR*, 2021.
- [54] Minwoo Byeon, Beomhee Park, Haecheon Kim, Sungjun Lee, Woonhyuk Baek, and Saehoon Kim. Coyo-700m: Image-text pair dataset. <https://github.com/kakaobrain/coyo-dataset>, 2022.
- [55] Alec Radford, Jong Wook Kim, Chris Hallacy, A. Ramesh, Gabriel Goh, Sandhini Agarwal, Girish Sastry, Amanda Askell, Pamela Mishkin, Jack Clark, Gretchen Krueger, and Ilya Sutskever. Learning transferable visual models from natural language supervision. In *ICML*, 2021.
- [56] Christoph Schuhmann, Romain Beaumont, Richard Vencu, Cade Gordon, Ross Wightman, Mehdi Cherti, Theo Coombes, Aarush Katta, Clayton Mullis, Mitchell Wortsman, et al. Laion-5b: An open large-scale dataset for training next generation image-text models. *Advances in Neural Information Processing Systems*, 35:25278–25294, 2022.
- [57] Hyungjin Chung, Jeongsol Kim, Michael T Mccann, Marc L Klasky, and Jong Chul Ye. Diffusion posterior sampling for general noisy inverse problems. *arXiv preprint arXiv:2209.14687*, 2022.
- [58] Lvmin Zhang, Anyi Rao, and Maneesh Agrawala. Adding conditional control to text-to-image diffusion models. In *Proceedings of the IEEE/CVF International Conference on Computer Vision*, pages 3836–3847, 2023.
- [59] Yutong He, Naoki Murata, Chieh-Hsin Lai, Yuhta Takida, Toshimitsu Uesaka, Dongjun Kim, Wei-Hsiang Liao, Yuki Mitsufuji, J Zico Kolter, Ruslan Salakhutdinov, et al. Manifold preserving guided diffusion. In *International Conference on Learning Representations*, 2023.
- [60] Diederik P Kingma and Jimmy Ba. Adam: A method for stochastic optimization. *arXiv preprint arXiv:1412.6980*, 2014.
- [61] Ken Shoemake. Animating rotation with quaternion curves. In *Proceedings of the 12th annual conference on Computer graphics and interactive techniques*, pages 245–254, 1985.
- [62] Hugo Touvron, Matthieu Cord, Matthijs Douze, Francisco Massa, Alexandre Sablayrolles, and Hervé Jégou. Training data-efficient image transformers & distillation through attention. In *International conference on machine learning*, pages 10347–10357. PMLR, 2021.
- [63] Mingxing Tan and Quoc Le. Efficientnet: Rethinking model scaling for convolutional neural networks. In *International conference on machine learning*, pages 6105–6114. PMLR, 2019.
- [64] Shengyu Zhao, Zhijian Liu, Ji Lin, Jun-Yan Zhu, and Song Han. Differentiable augmentation for data-efficient gan training. *Advances in neural information processing systems*, 33:7559–7570, 2020.
- [65] Liyuan Liu, Haoming Jiang, Pengcheng He, Weizhu Chen, Xiaodong Liu, Jianfeng Gao, and Jiawei Han. On the variance of the adaptive learning rate and beyond. *arXiv preprint arXiv:1908.03265*, 2019.
- [66] James Betker, Gabriel Goh, Li Jing, Tim Brooks, Jianfeng Wang, Linjie Li, Long Ouyang, Juntang Zhuang, Joyce Lee, Yufei Guo, et al. Improving image generation with better captions. *Computer Science*. <https://cdn.openai.com/papers/dall-e-3.pdf>, 2(3):8, 2023.
- [67] Haotian Liu, Chunyuan Li, Qingyang Wu, and Yong Jae Lee. Visual instruction tuning. *Advances in neural information processing systems*, 36, 2024.
- [68] Mathilde Caron, Hugo Touvron, Ishan Misra, Hervé Jégou, Julien Mairal, Piotr Bojanowski, and Armand Joulin. Emerging properties in self-supervised vision transformers. In *Proceedings of the IEEE/CVF international conference on computer vision*, pages 9650–9660, 2021.

- [69] Tim Dettmers, Mike Lewis, Sam Shleifer, and Luke Zettlemoyer. 8-bit optimizers via block-wise quantization. *arXiv preprint arXiv:2110.02861*, 2021.
- [70] Adrien Saumard and Jon A Wellner. Log-concavity and strong log-concavity: a review. *Statistics surveys*, 8:45, 2014.
- [71] Wenpin Tang and Hanyang Zhao. Contractive diffusion probabilistic models. *arXiv preprint arXiv:2401.13115*, 2024.
- [72] Junlong Lyu, Zhitang Chen, and Shoubo Feng. Sampling is as easy as keeping the consistency: convergence guarantee for consistency models. 2023.
- [73] Xuefeng Gao, Hoang M Nguyen, and Lingjiong Zhu. Wasserstein convergence guarantees for a general class of score-based generative models. *arXiv preprint arXiv:2311.11003*, 2023.
- [74] Bernard A Asner, Jr. On the total nonnegativity of the hurwitz matrix. *SIAM Journal on Applied Mathematics*, 18(2):407–414, 1970.
- [75] Nam Parshad Bhatia and Giorgio P Szegő. *Stability theory of dynamical systems*. Springer Science & Business Media, 2002.
- [76] Lars Mescheder, Sebastian Nowozin, and Andreas Geiger. The numerics of gans. *Advances in neural information processing systems*, 30, 2017.
- [77] David Balduzzi, Sebastien Racaniere, James Martens, Jakob Foerster, Karl Tuyls, and Thore Graepel. The mechanics of n-player differentiable games. In *International Conference on Machine Learning*, pages 354–363. PMLR, 2018.
- [78] Ian Gemp and Sridhar Mahadevan. Global convergence to the equilibrium of gans using variational inequalities. *arXiv preprint arXiv:1808.01531*, 2018.
- [79] Chuang Wang, Hong Hu, and Yue Lu. A solvable high-dimensional model of gan. *Advances in Neural Information Processing Systems*, 32, 2019.
- [80] Chongli Qin, Yan Wu, Jost Tobias Springenberg, Andy Brock, Jeff Donahue, Timothy Lillicrap, and Pushmeet Kohli. Training generative adversarial networks by solving ordinary differential equations. *Advances in Neural Information Processing Systems*, 33:5599–5609, 2020.

# Contents

<b>1</b>	<b>Introduction</b>	<b>2</b>
<b>2</b>	<b>Preliminary and Related Works</b>	<b>2</b>
<b>3</b>	<b>Progressive Growing of Diffusion Autoencoder</b>	<b>3</b>
3.1	Objective Function . . . . .	3
3.2	Progressively Growing Decoder for Higher Resolution . . . . .	4
3.3	Optimality Guarantee and Training Stability . . . . .	4
<b>4</b>	<b>PaGoDA with Classifier-Free Guidance</b>	<b>5</b>
4.1	Classifier-Free GAN . . . . .	5
4.2	Objective Function with Classifier-Free Guidance . . . . .	5
<b>5</b>	<b>Experiments</b>	<b>6</b>
5.1	Class-Conditional ImageNet Generation . . . . .	6
5.2	Controlled Model Analysis . . . . .	7
5.3	Text-to-Image Generation . . . . .	8
5.4	Applications: Controllable Generation and Inverse Problems . . . . .	9
<b>6</b>	<b>Conclusion</b>	<b>10</b>
<b>A</b>	<b>Experimental Details</b>	<b>17</b>
A.1	Conditional Generation with ImageNet . . . . .	17
A.2	Text-to-Image Generation . . . . .	18
<b>B</b>	<b>Theoretical Analysis</b>	<b>20</b>
B.1	Convergence with PaGoDA’s Reconstruction Loss . . . . .	20
B.1.1	Preliminaries of Convergence Analysis . . . . .	20
B.1.2	$W_2$ Bound with PaGoDA’s Reconstruction Loss . . . . .	21
B.1.3	$W_1$ Bound with PaGoDA’s Reconstruction Loss . . . . .	25
B.2	Optimality analysis . . . . .	27
B.3	Stability Analysis . . . . .	28
B.3.1	Preliminaries of Dynamical System . . . . .	28
B.3.2	Preliminaries for Analysis of PaGoDA Training . . . . .	29
B.3.3	PaGoDA’s Training is Stable . . . . .	30
B.3.4	Literature on Stability Analysis of Adversarial Training . . . . .	33



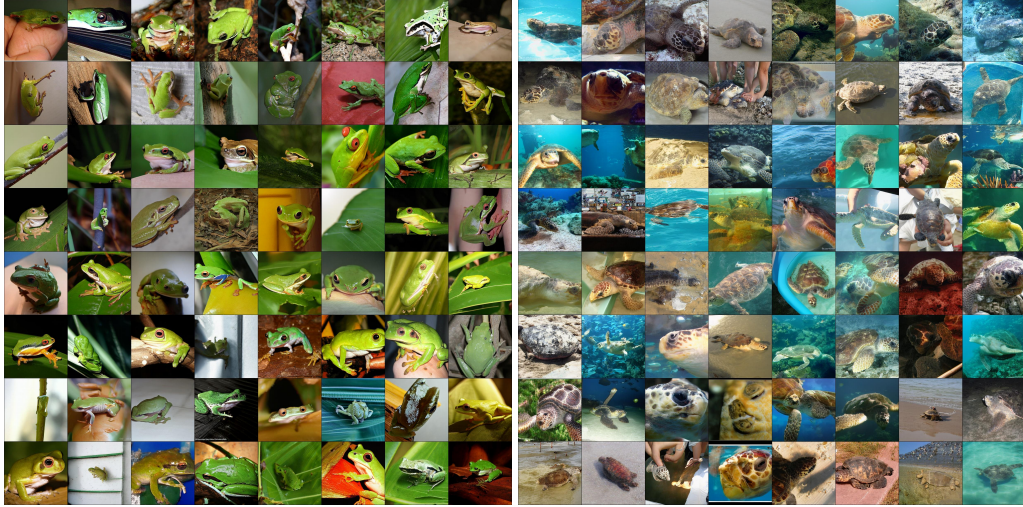


Figure 8: Uncurated samples generated by PaGoDA at resolution  $512^2$ . Left: class 31 (tree frog); Right: class 33 (loggerhead turtle).

## A Experimental Details

### A.1 Conditional Generation with ImageNet

Throughout the experiments, we omit the class condition  $c$  otherwise mentioned for notational simplicity.

**Dataset Construction.** We loaded ImageNet2014<sup>3</sup> dataset using center cropping and downsampling using the bicubic algorithm from the PIL python package. To augment the data, we applied a horizontal random flip, and obtained each of latent representations by solving the EDM’s 2nd-order ODE sampler (Heun’s method) [40] with their suggested diffusion time scheduling and timestep selection. Consequently, in total, we processed approximately 2.5 million data instances forward in time using the PF-ODE to prepare for training. This computational cost of constructing the training dataset is comparable to sampling an equivalent volume of sample from a pre-trained diffusion model.

**GAN Details.** We adopted the discriminator architecture from StyleGAN-XL. Initially, We loaded DeiT-base [62] and EfficientNet-lite [63] as feature extractors, in line with StyleGAN-XL’s setup. When processing real or fake data through the discriminator, we first applied differentiable augmentation (DiffAugment) [64], incorporating three transformations: *Translation*, *Cutout*, and *Color*. Interestingly, we observed no performance differences between the *unconditional* and *conditional* discriminators. We hypothesize that this lack of disparity arises because the discriminator primarily updates the generator to refine high-frequency details, while preserving the low-frequency global semantics due to the reconstruction power. Additionally, we opted not to use additional techniques to tame the GAN training, such as R1 regularization [27] or path length regularization [26] in our GAN training. PaGoDA’s training generally remains stable due to its reconstruction loss, which is consistent with our theoretical expectation (Theorem B.9).

We conducted tests on GANs under two distinct scenarios. Initially, following the approach used in Stable Diffusion’s VAE training, we introduced both the real data  $\mathbf{x}$  and the reconstructed sample  $\tilde{\mathbf{x}} = G_{\theta}(E(\mathbf{x}))$  to the discriminator, training it to differentiate between the two while updating the generator to maximize  $\log D_{\psi}(\tilde{\mathbf{x}})$ . In this setup, as the reconstruction only utilizes the latent representation  $E(\mathbf{x})$ , the generation quality is not improved.

In the second scenario, adhering to the traditional GAN framework, we trained the discriminator using randomly sampled real data alongside randomly generated fake data  $\tilde{\mathbf{x}} = G_{\theta}(\mathbf{z})$  from  $\mathbf{z} \sim p_{\text{prior}}(\mathbf{z})$ . Then, the endeavor of maximizing  $\log D_{\psi}(\tilde{\mathbf{x}})$  now significantly improves the generation quality. Overall, we observed no performance degradation when both types of GAN training were applied to

<sup>3</sup><https://www.image-net.org/index.php>

- You are LLaVA, a large language and vision assistant trained by UW Madison WAIV Lab.
- You are able to understand the visual content that the user provides, and assist the user with a variety of tasks using natural language.
- You should follow the instructions carefully and explain your answers in detail.
- Given the caption of this image "{text prompt}", describe this image in a very detailed manner

Figure 9: Input prompt of LLaVA to recaption the text-image paired data.

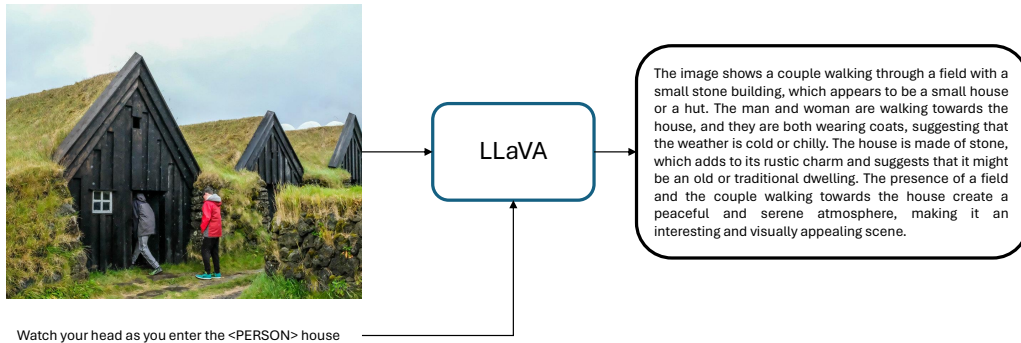


Figure 10: Example of recaptioned image-text pair.

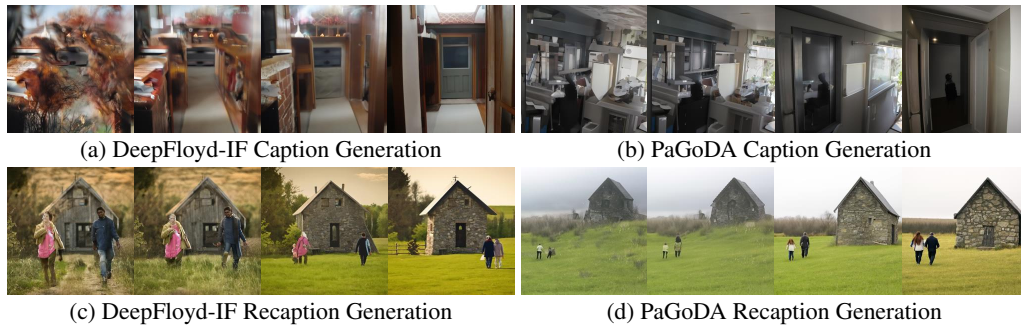


Figure 11: Caption vs. Recaption. From left to right, CFG scale increases. The caption and its corresponding recaption are given by the exemplary case in Figure 10.

the generator. However, given our limited budget and the goal to develop a generative model rather than a compression model, we opted to proceed solely with the second type of GAN setup.

**Reconstruction Details.** For the reconstruction loss, we train the generator  $G_\theta$  by comparing the original data  $\mathbf{x} \sim p_{\text{data}}(\mathbf{x})$  and its reconstructed counterpart  $G_\theta(E(\mathbf{x}, \mathbf{c}), \mathbf{c})$  at the data’s resolution. Since our training occurs in pixel space, we conduct this comparison in the feature space using the Learned Perceptual Image Patch Similarity (LPIPS) metric, and there is no need to develop a new feature extractor in latent space. We experimented with features extracted from DeiT-base [62] and EfficientNet-lite [63]; however, we observed no notable improvement from using LPIPS.

For the training, we use the RAdam [65] with learning rate of  $8e-6$  for the decoder and  $2e-3$  for the discriminator, and without weight decay. We use the EMA of 0.999, and all reported FIDs are based on the EMA checkpoint. Until  $256^2$  resolution, we use only 1 H100 node (with 80Gb memory) to train, and we use 8 A100 nodes (with 40Gb memory, in total  $8 \times 8 = 64$  GPUs) to train the  $512^2$  model. Throughout the experiments, we use the batch size of 256.

Figures 8 illustrate random samples of PaGoDA at  $512^2$  resolution.

## A.2 Text-to-Image Generation

**Dataset Construction.** Due to the presence of inappropriate contents (CSAM) in the LAION dataset [56], we have decided to discontinue its use. Instead, we are now training our model using the CC12M [53] and a filtered version of COYO-700M [54] datasets. For COYO-700M, we apply filters to select only those text-image pairs that meet specific criteria: a CLIP score (measured by ViT-B/32 [55]) above 32.0 and an aesthetic score-v2 [56] higher than 5.0. Additionally, we are enhancing

the dataset quality by recaptioning the original text prompts from CC12M, adopting practices similar to those used in DallE-3 [66] and PixArt- $\alpha$  [47]. Specifically, we employ LLaVA-7B [67], a language model with vision assistance, to generate descriptions of the images based on the text prompts, thereby ensuring more relevant and accurate text-image pairings.

The input prompt of LLaVA is depicted in Figure 9, where we put text prompt to  $\{\text{text prompt}\}$ . The output from this recaptioning process adheres to a consistent format, typically beginning with phrases like “This image features ...” or “This image shows ...”. To provide clear demonstration, Figure 11 displays several examples of original captions alongside their recaptioned counterparts.

Interestingly, the recaptioned samples generally outperform the original caption samples. Notably, the recaptioned samples exhibit sufficient quality, particularly when the CFG scale is small, as shown in Figure 12. Therefore, to ensure balanced generation performance across varying CFG scales, we generate samples from the original captions with the CFG scale uniformly sampled from the range [2, 10]. For the recaptioned text, we use a CFG scale that follows a truncated Gaussian distribution on the range [1, 10], centered at 2 with a scale of 3. Overall, incorporating these recaptioned texts into the PaGoDA training results in only a marginal improvement in performance metrics such as FID and CLIP. However, it significantly enhances the actual quality of generation, particularly at smaller CFG scales, because the recaptioning provides better-aligned training data.

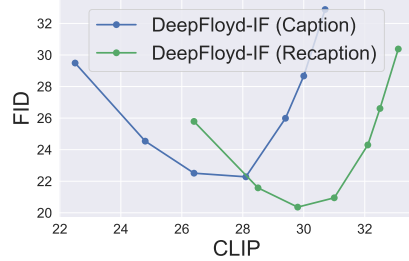


Figure 12: Effect of recaptioning.

Using LLaVA, we recaption  $\tilde{c}(x, c)$  and obtain the DDIM latent representation,  $E(x, \tilde{c}(x, c))$ , on the entire CC12M dataset. Then, for the original text  $c$ , we have a triplet of (image, text, latent) of  $(x, c, E(x, c))$  for one set, and another triplet  $(x, \tilde{c}(x, c), E(x, \tilde{c}(x, c)))$  for recaptioned dataset. When computing  $\mathcal{L}_{rec}$ , we mix these triplets and randomly sample from this mixed dataset.

**GAN Details.** Similar to the ImageNet case, we have adopted the discriminator architecture from StyleGAN-T. In line with StyleGAN-T, we utilize the DINO ViT-S/16 [68] as the feature extractor and apply DiffAugment [64], incorporating *Translation*, *Cutout*, and *Color* transformations. Building upon this architecture, we integrate a  $\omega$  condition into each discriminator head, as illustrated in Figure 13. The inputs for each discriminator head include the DINO feature, text CLIP embedding, and the CFG scale  $\omega$ , which is scaled by a factor of 100. We handle the CFG scale similarly to the time variable in traditional diffusion

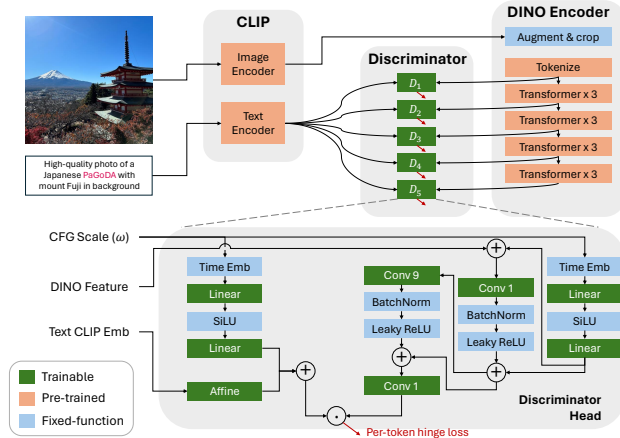


Figure 13: Discriminator architecture.

U-Net models, incorporating the output CFG embedding into the existing components of the StyleGAN-T discriminator head. We assume both image  $x$  and text  $c$  are related with the CFG scale, thus we designed the discriminator to incorporate  $\omega$  information into both modules, enhancing the relevance and contextuality of the discrimination process.

**Reconstruction Details.** In our text-to-image training, we largely adhere to the protocols established for ImageNet training. However, a notable modification involves the decoder network, which now incorporates a  $\omega$  condition as an auxiliary input. Crucially, this  $\omega$  condition is processed in decoder in the same way as the time condition in diffusion models. We achieve this by scaling  $\omega$  by a factor of 100, thus aligning it with the existing time ranges. This method ensures a consistent treatment of the  $\omega$  parameter, integrating it smoothly into the established model architecture.

**CLIP Details.** Neither the reconstruction loss nor the GAN loss directly models or maximizes the text-image correlation. To address this, we introduce an additional text-image alignment metric to

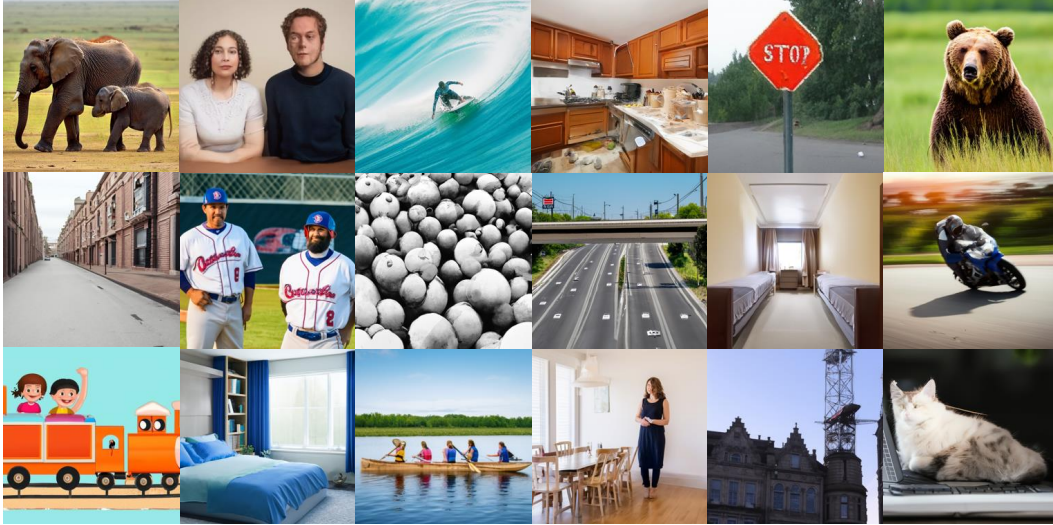


Figure 15: Text-to-image samples from PaGoDA.

train our model. Specifically, we employ ViT-L/14 [55] to assess the CLIP value. This regularization significantly enhances PaGoDA’s performance, as evidenced in Figure 14 by improving both FID and CLIP scores. These enhancements suggest that not only is the sample quality improving, but also the alignment between text and images is becoming more accurate.

For the training, we use the AdamW8bit optimizer [69] to minimize the required memory with learning rate of  $1e-5$  for both decoder and discriminator. Similar to the ImageNet experiment, we do not apply the weight decay. In this text-to-image experiment, we do not use EMA, following previous works [23]. In the base resolution, we use the adaptive weighting with  $\lambda = 4 \frac{\|\nabla_{\theta^l} (\mathcal{L}_{rec} + \mathcal{L}_{dcl}^{CFG})\|_2^2}{\|\nabla_{\theta^l} \mathcal{L}_{adv}^{CFG}\|_2^2}$ . Overall, we use the DeepFloyd-IF-I model with 0.9B number of parameters.

Figure 15 illustrates more samples from PaGoDA with  $256^2$  resolution.

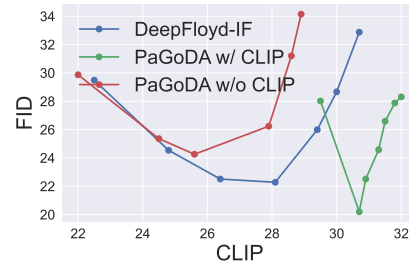


Figure 14: Effect of CLIP regularization.

## B Theoretical Analysis

In this section, we present rigorous statements and proofs of all theorems. The theorems are shown for the unconditional generation case (i.e., without the condition  $c$ ), but the analysis can be extended to the conditional scenario.

### B.1 Convergence with PaGoDA’s Reconstruction Loss

In Section B.1.1, we introduce the necessary notations and preliminaries. In Sections B.1.2 and B.1.3, we demonstrate that the Wasserstein-1 and Wasserstein-2 discrepancies of the learned density (with PaGoDA’s reconstruction loss) from  $p_{data}$  are upper bounded by PaGoDA’s reconstruction loss and the pre-trained DM’s training error. All results are proved for unconditional generation (i.e., without  $c$  as an input), but they can be easily generalized to the conditional case.

#### B.1.1 Preliminaries of Convergence Analysis

Consider OU process for  $t \in [0, T]$ , where  $T > 0$ :

$$dx_t = -f(t)x_t dt + g(t) dw_t$$

Its associated PF-ODE is

$$d\mathbf{x}_t = \left[ -f(t)\mathbf{x}_t - \frac{1}{2}g^2(t)\nabla \log p_t(\mathbf{x}_t) \right] dt.$$

We consider  $f(t) \equiv 1$  and  $g(t) \equiv \sqrt{2}$  for simplicity. That is,

$$d\mathbf{x}_t = -\mathbf{x}_t dt + \sqrt{2} d\mathbf{w}_t. \quad (4)$$

We recall that PaGoDA's reconstruction loss (unconditional case) is defined as:

$$\mathcal{L}_{\text{rec}}(\boldsymbol{\theta}; \phi_0) := \mathbb{E}_{p_{\text{data}}(\mathbf{x})p_{\phi_0}(\mathbf{z}|\mathbf{x})} \left[ \|\mathbf{x} - G_{\boldsymbol{\theta}}^{T \rightarrow 0}(\mathbf{z})\|_2^2 \right],$$

Here, we use  $p_{\phi_0}(\mathbf{z}|\mathbf{x})$  to denote the density obtained by solving the pre-trained teacher DM's empirical PF-ODE forward in time from  $t = 0$  to  $t = T$ :

$$d\mathbf{x}_t = \left[ -f(t)\mathbf{x}_t - \frac{1}{2}g^2(t)\mathbf{s}_{\phi_0}(\mathbf{x}_t, t) \right] dt,$$

where  $\mathbf{s}_{\phi_0}(\mathbf{x}_t, t)$  indicates the pre-trained DM. We remark that  $p_{\phi_0}(\mathbf{z}|\mathbf{x})$  defines a deterministic process.

We take  $p_{\text{prior}} := \mathcal{N}(\mathbf{0}, (1 - e^{-2T})\mathbf{I})$  as the prior distribution, and define  $p_{T, \phi_0} := G_{\phi_0}^{0 \rightarrow T} \# p_{\text{data}}$  as the distribution obtained by solving the teacher-determined empirical PF-ODE forward in time. Let us consider the density obtained by sampling from PaGoDA (trained without GAN)  $p_{0, \theta} := G_{\theta}^{T \rightarrow 0} \# p_{\text{prior}}$ . We also let  $G^{T \rightarrow 0}$  denote the ground truth transition map from  $T$  to 0, defined by the PF-ODE.

Conceptually, Theorems B.1 and B.3 demonstrate that

$$W_p(p_{0, \theta}, p_{\text{data}}) \lesssim \mathcal{L}_{\text{rec}}(\boldsymbol{\theta}; \phi_0) + \epsilon_{\text{DM}}, \quad p = 1, 2.$$

This implies that training with PaGoDA's reconstruction loss ensures the learned density  $p_{0, \theta} = G_{\theta}^{T \rightarrow 0} \# p_{\text{prior}}$  is close to  $p_{\text{data}}$  in Wasserstein distance sense. Moreover, improving the teacher DM to reduce the error  $\epsilon_{\text{DM}}$  is a way to further decrease the discrepancy between  $p_{0, \theta}$  and  $p_{\text{data}}$ .

We remark that the differences between the two theorems primarily lie in the distinct smoothness assumptions on  $p_{\text{data}}$ .

### B.1.2 $W_2$ Bound with PaGoDA's Reconstruction Loss

**Assumption I-1.** (i)  $m^2 := \mathbb{E}_{p_{\text{data}}(\mathbf{x})} \|\mathbf{x}\|_2^2 < \infty$ ;

(ii) There is a  $\epsilon_{\text{DSM}} > 0$  so that  $\sup_{\mathbf{x}, t} \|\mathbf{s}_{\phi_0}(\mathbf{x}, t) - \nabla \log p_t(\mathbf{x})\|_2^2 \leq \epsilon_{\text{DSM}}^2$ ;

(iii)  $G_{\theta}^{T \rightarrow 0}$  is Lipschitz in  $\mathbf{x}$ :

$$\Lambda := \sup_{\mathbf{x} \neq \mathbf{y}} \frac{\|G_{\theta}^{T \rightarrow 0}(\mathbf{x}) - G_{\theta}^{T \rightarrow 0}(\mathbf{y})\|_2}{\|\mathbf{x} - \mathbf{y}\|_2} < \infty,$$

for all  $\boldsymbol{\theta}$  and  $T$ .

(iv)  $\log p_{\text{data}}$  is  $\gamma$ -strongly concave with  $\gamma > 3/2$ :

$$\langle \mathbf{x} - \mathbf{y}, \nabla \log p_{\text{data}}(\mathbf{x}) - \nabla \log p_{\text{data}}(\mathbf{y}) \rangle \leq -\gamma \|\mathbf{x} - \mathbf{y}\|_2^2,$$

for all  $\mathbf{x}$  and  $\mathbf{y}$ .

**Theorem B.1.** *Given that Assumption I-1 holds, suppose  $\delta$  is a positive constant such that  $\delta < \frac{e^{-2T}}{3 - e^{-2T}}$ , and let  $h(\gamma, T) := \frac{\gamma}{e^{-2T} + \gamma(1 - e^{-2T})} - (1 + \delta)$ , where it is noted that  $h(\gamma, T)$  is also positive. Then*

$$\begin{aligned} W_2(p_{0, \theta}, p_{\text{data}}) &\leq \mathcal{L}_{\text{rec}}(\boldsymbol{\theta}; \phi_0) + \left[ \mathbb{E}_{p_{\text{data}}(\mathbf{x})p_{\phi_0}(\mathbf{z}|\mathbf{x})} \|\mathbf{x} - G^{T \rightarrow 0}(\mathbf{z})\|_2^2 \right]^{\frac{1}{2}} \\ &\quad + (\Lambda + e^{-\frac{1}{2}h(\gamma, T)T}) W_2(p_T, p_{T, \phi_0}) \end{aligned}$$

$$+ \frac{\epsilon_{DM}}{\sqrt{2\delta h(\gamma, T)}} (1 - e^{-h(\gamma, T)T})^{\frac{1}{2}} + e^{-\frac{T}{2}} m\Lambda.$$

In particular, if we assume Assumption I-1 (iii) holds also for  $G^{T \rightarrow 0}$ ,

$$W_2(p_{0, \theta}, p_{data}) \lesssim \mathcal{L}_{rec}(\theta; \phi_0) + \epsilon_{DM} + e^{-\frac{T}{2}} m\Lambda.$$

Here, we use  $\lesssim$  to absorb the dependence on the constants  $T$  and  $\gamma$  into the inequality.

We present an inequality which is essential for the proof of Theorem B.1.

**Lemma B.2** (Proposition 3.5. in [70]). *Let  $P$  and  $Q$  be two distributions on  $\mathbb{R}^D$ . Suppose that  $\log P$  is  $\gamma_P$ -concave and  $\log Q$  is  $\gamma_Q$ -concave. Then the convolution of  $\log P * Q$  is a  $(1/\gamma_P + 1/\gamma_Q)^{-1}$ -concave distribution.*

**Proof of Theorem B.1.** The proof of the theorem is inspired by [71, 72]. Define  $p_{T, \phi_0} := G_{\phi_0}^{0 \rightarrow T} \# p_{data}$ , and  $p_{0, \phi_0} := G^{T \rightarrow 0} \# p_{T, \phi_0}$ . From the triangle inequality, we have

$$W_2(p_{0, \theta}, p_{data}) \leq \underbrace{W_2(p_{0, \theta}, p_{0, \phi_0})}_{(A)} + \underbrace{W_2(p_{0, \phi_0}, p_{data})}_{(B)}.$$

For (A), let  $\pi(\mathbf{y}, \mathbf{z}) \in \Pi(p_{prior}, p_{T, \phi_0})$  be a coupling of  $p_{prior}$  and  $p_{T, \phi_0}$ . Then

$$\begin{aligned} (A) &= W_2(G_{\theta}^{T \rightarrow 0} \# p_{prior}, G^{T \rightarrow 0} \# p_{T, \phi_0}) \\ &\leq \left( \mathbb{E}_{(\mathbf{y}, \mathbf{z}) \sim \pi} \|G_{\theta}^{T \rightarrow 0}(\mathbf{y}) - G^{T \rightarrow 0}(\mathbf{z})\|_2^2 \right)^{\frac{1}{2}} \\ &\leq \underbrace{\left( \mathbb{E}_{(\mathbf{y}, \mathbf{z}) \sim \pi} \|G_{\theta}^{T \rightarrow 0}(\mathbf{y}) - G_{\theta}^{T \rightarrow 0}(\mathbf{z})\|_2^2 \right)^{\frac{1}{2}}}_{(A.1)} + \underbrace{\left( \mathbb{E}_{(\mathbf{y}, \mathbf{z}) \sim \pi} \|G_{\theta}^{T \rightarrow 0}(\mathbf{z}) - G^{T \rightarrow 0}(\mathbf{z})\|_2^2 \right)^{\frac{1}{2}}}_{(A.2)}. \end{aligned}$$

For (A.1), we can yield

$$\begin{aligned} (A.1) &\leq \Lambda \min_{\pi \in \Pi(p_{prior}, p_{T, \phi_0})} \left( \mathbb{E}_{(\mathbf{y}, \mathbf{z}) \sim \pi} \|\mathbf{y} - \mathbf{z}\|_2^2 \right)^{\frac{1}{2}} \\ &= \Lambda W_2(p_{prior}, p_{T, \phi_0}) \\ &\leq \Lambda W_2(p_{prior}, p_T) + \Lambda W_2(p_T, p_{T, \phi_0}) \\ &\leq e^{-\frac{T}{2}} \left( \mathbb{E}_{p_{data}(\mathbf{x}_0)} \|\mathbf{x}_0\|_2^2 \right)^{\frac{1}{2}} \Lambda + \Lambda W_2(p_T, p_{T, \phi_0}). \end{aligned} \quad (5)$$

Here, the last inequality is a consequence of the following bound

$$W_2(p_{prior}, p_T) \leq e^{-\frac{T}{2}} \left( \mathbb{E}_{p_{data}(\mathbf{x}_0)} \|\mathbf{x}_0\|_2^2 \right)^{\frac{1}{2}},$$

which holds because  $p_{prior}$  is taken as  $\mathcal{N}(\mathbf{0}, (1 - e^{-2T})\mathbf{I})$ , and  $\mathbf{x}_T \sim p_T$  governed by Eq. (4) admits the expression

$$\mathbf{x}_T = e^{-T} \mathbf{x}_0 + \int_0^T e^{-(T-s)} \sqrt{2} d\mathbf{w}_s = e^{-T} \mathbf{x}_0 + \mathbf{z}, \quad \mathbf{z} \sim \mathcal{N}(\mathbf{0}, (1 - e^{-2T})\mathbf{I}).$$

For (A.2), since  $p_{T, \phi_0}(\mathbf{z}) = \int p_{\phi_0}(\mathbf{z}|\mathbf{x}) p_{data}(\mathbf{x}) d\mathbf{x}$ , by applying Minkowski inequality we have

$$\begin{aligned} (A.2) &= \left( \mathbb{E}_{(\mathbf{y}, \mathbf{z}) \sim \pi} \|G_{\theta}^{T \rightarrow 0}(\mathbf{z}) - G^{T \rightarrow 0}(\mathbf{z})\|_2^2 \right)^{\frac{1}{2}} \\ &= \left( \mathbb{E}_{\mathbf{z} \sim p_{T, \phi_0}(\mathbf{z})} \|G_{\theta}^{T \rightarrow 0}(\mathbf{z}) - G^{T \rightarrow 0}(\mathbf{z})\|_2^2 \right)^{\frac{1}{2}} \\ &\leq \left( \mathbb{E}_{p_{data}(\mathbf{x}) p_{\phi_0}(\mathbf{z}|\mathbf{x})} \|G_{\theta}^{T \rightarrow 0}(\mathbf{z}) - \mathbf{x}\|_2^2 \right)^{\frac{1}{2}} + \left( \mathbb{E}_{p_{data}(\mathbf{x}) p_{\phi_0}(\mathbf{z}|\mathbf{x})} \|\mathbf{x} - G^{T \rightarrow 0}(\mathbf{z})\|_2^2 \right)^{\frac{1}{2}} \\ &= \mathcal{L}_{rec}(\theta; \phi_0) + \left[ \mathbb{E}_{p_{data}(\mathbf{x}) p_{\phi_0}(\mathbf{z}|\mathbf{x})} \|\mathbf{x} - G^{T \rightarrow 0}(\mathbf{z})\|_2^2 \right]^{\frac{1}{2}}. \end{aligned} \quad (6)$$

The proof for (B) is motivated by [71]. Consider the following two reverse time PF-ODEs on the interval  $[0, T]$

$$\frac{d\hat{\mathbf{z}}_{t,\phi_0}}{dt} = \hat{\mathbf{z}}_{t,\phi_0} + \mathbf{s}_{\phi_0}(\hat{\mathbf{z}}_{t,\phi_0}, T-t), \quad \hat{\mathbf{z}}_{0,\phi_0} \sim p_{T,\phi_0}$$

and

$$\frac{d\hat{\mathbf{z}}_t}{dt} = \hat{\mathbf{z}}_t + \nabla \log p_{T-t}(\hat{\mathbf{z}}_t), \quad \hat{\mathbf{z}}_0 \sim p_T,$$

with a coupling of  $\hat{\mathbf{z}}_{0,\phi_0} \sim p_{T,\phi_0}$  and  $\hat{\mathbf{z}}_0 \sim p_T$  so that  $W_2^2(p_{T,\phi_0}, p_T) = \mathbb{E} \|\hat{\mathbf{z}}_{0,\phi_0} - \hat{\mathbf{z}}_0\|_2^2$ . We notice that  $W_2^2(p_{0,\phi_0}, p_{\text{data}}) \leq \mathbb{E} \|\hat{\mathbf{z}}_{T,\phi_0} - \hat{\mathbf{z}}_T\|_2^2$ . Thus, we need to obtain an upper bound of  $\mathbb{E} \|\hat{\mathbf{z}}_{T,\phi_0} - \hat{\mathbf{z}}_T\|_2^2$ . Let  $u(t) := \mathbb{E} \|\hat{\mathbf{z}}_{t,\phi_0} - \hat{\mathbf{z}}_t\|_2^2$ . Then

$$\begin{aligned} \frac{d}{dt} u(t) &= 2\mathbb{E} \langle \hat{\mathbf{z}}_{t,\phi_0} - \hat{\mathbf{z}}_t, \frac{d}{dt} (\hat{\mathbf{z}}_{t,\phi_0} - \hat{\mathbf{z}}_t) \rangle \\ &= 2u(t) + 2\mathbb{E} \left[ \langle \hat{\mathbf{z}}_{t,\phi_0} - \hat{\mathbf{z}}_t, \mathbf{s}_{\phi_0}(\hat{\mathbf{z}}_{t,\phi_0}, T-t) - \nabla \log p_{T-t}(\hat{\mathbf{z}}_t) \rangle \right] \\ &= 2u(t) + 2\mathbb{E} \left[ \underbrace{\langle \hat{\mathbf{z}}_{t,\phi_0} - \hat{\mathbf{z}}_t, \mathbf{s}_{\phi_0}(\hat{\mathbf{z}}_{t,\phi_0}, T-t) - \nabla \log p_{T-t}(\hat{\mathbf{z}}_{t,\phi_0}) \rangle}_{(B.1)} \right] \\ &\quad + 2\mathbb{E} \left[ \underbrace{\langle \hat{\mathbf{z}}_{t,\phi_0} - \hat{\mathbf{z}}_t, \nabla \log p_{T-t}(\hat{\mathbf{z}}_{t,\phi_0}) - \nabla \log p_{T-t}(\hat{\mathbf{z}}_t) \rangle}_{(B.2)} \right]. \end{aligned} \quad (7)$$

Let  $\delta > 0$ , by applying Yang's inequality  $ab = (\sqrt{2\delta}a)(\frac{b}{\sqrt{2\delta}}) \leq \delta a^2 + \frac{b^2}{4\delta}$  to (B.1) for nonnegative  $a$  and  $b$ , and the Assumption I-1, it becomes

$$(B.1) \leq \delta u(t) + \frac{\epsilon_{\text{DM}}^2}{4\delta}. \quad (8)$$

We turn our attention to (B.2). Naively, (B.2) may be naively bounded above by  $\text{Lip}(\nabla \log p_t(\cdot))u(t)$ , where  $\text{Lip}(\nabla \log p_t(\cdot))$  is the Lipschitz constant of  $\nabla \log p_t(\cdot)$  in  $\mathbf{x}$ . However, we will now derive a sharper bound by incorporating assumptions on the data distribution.

We notice that  $p_t(\mathbf{x}_t) = \int p_{t|0}(\mathbf{x}_t|\mathbf{x}_0)p_{\text{data}}(\mathbf{x}_0) d\mathbf{x}_0$ , where  $p_{t|0}(\mathbf{x}_t|\mathbf{x}_0) = \mathcal{N}(\mathbf{x}_t; e^{-t}\mathbf{x}_0, (1 - e^{-2t})\mathbf{I})$  is a transition kernel from 0 to  $t$  determined by the forward SDE. Therefore, expressing  $p_t$  in convolution form, under Assumption I-1, and leveraging Lemma B.2, we deduce that  $\log p_{T-t}$  is a  $\gamma/(e^{-2(T-t)} + \gamma(1 - e^{-2(T-t)}))$ -strongly concave distribution (see [73]). Hence,

$$(B.2) \leq -\frac{\gamma}{e^{-2(T-t)} + \gamma(1 - e^{-2(T-t)})} u(t). \quad (9)$$

With the inequalities (8) and (9), we deduce from Eq. (7) that

$$u'(t) \leq a(t)u(t) + \frac{\epsilon_{\text{DM}}^2}{2\delta}, \quad \text{where } a(t) := \left( 2 + 2\delta - \frac{2\gamma}{e^{-2(T-t)} + \gamma(1 - e^{-2(T-t)})} \right).$$

By applying Grönwall's inequality, we obtain

$$\begin{aligned} \mathbb{E} \|\hat{\mathbf{z}}_{T,\phi_0} - \hat{\mathbf{z}}_T\|_2^2 &\leq e^{A(T)} \mathbb{E} \|\hat{\mathbf{z}}_{0,\phi_0} - \hat{\mathbf{z}}_0\|_2^2 + \frac{\epsilon_{\text{DM}}^2}{2\delta} \int_0^T e^{A(T)-A(t)} dt, \\ &= e^{A(T)} W_2^2(p_{T,\phi_0}, p_T) + \frac{\epsilon_{\text{DM}}^2}{2\delta} \int_0^T e^{A(T)-A(t)} dt. \end{aligned} \quad (10)$$

where  $A(t) := \int_0^t a(s) ds$ .

We aim to find an upper bound for inequality (10) that decays exponentially with respect to  $T$ . In  $a(t)$ ,  $b(t) := \frac{\gamma}{e^{-2(T-t)} + \gamma(1 - e^{-2(T-t)})}$  as a function of  $t$  has the derivative as  $\frac{2\gamma(\gamma-1)e^{-2(T-t)}}{(e^{-2(T-t)} + \gamma(1 - e^{-2(T-t)}))^2}$ .

This implies when  $\gamma \geq 1$ ,  $b$ 's minimum occurs at  $b(0) = \frac{\gamma}{\gamma + e^{-2T}(1-\gamma)}$ , which implies  $a(t) \leq 2(1 + \delta - b(0))$  for all  $t \in [0, T]$ . Setting  $\delta < \frac{e^{-2T}}{3 - e^{-2T}}$ , which implies  $\frac{1}{2} > \frac{\delta}{(1+\delta)e^{-2T} - \delta}$ , then  $\gamma > \frac{3}{2} = 1 + \frac{1}{2} > 1 + \frac{\delta}{(1+\delta)e^{-2T} - \delta}$  (notice that  $(1 + \delta)e^{-2T} - \delta > 2\delta$ ), we can deduce that

$$a(t) \leq 1 + \delta - \frac{\gamma}{e^{-2T} + \gamma(1 - e^{-2T})} < 0.$$

Let  $h(\gamma, T) := \frac{\gamma}{e^{-2T} + \gamma(1 - e^{-2T})} - (1 + \delta) > 0$ . Then we establish that  $a(t) \leq -h(\gamma, T)$ ,  $A(T) \leq -h(\gamma, T)T$ , and  $A(T) - A(t) \leq -h(\gamma, T)t$  which implies  $\int_0^T e^{A(T)-A(t)} dt \leq 1 - e^{-h(\gamma, T)T}$ . By applying the above bounds and inequality (10), (B) becomes

$$\begin{aligned} (B) &\leq \left( \mathbb{E} \|\hat{\mathbf{z}}_{T, \phi_0} - \hat{\mathbf{z}}_T\|_2^2 \right)^{\frac{1}{2}} \\ &\leq \left( e^{-h(\gamma, T)T} W_2^2(p_{T, \phi_0}, p_T) + \frac{\epsilon_{\text{DM}}^2}{2\delta h(\gamma, T)} (1 - e^{-h(\gamma, T)T}) \right)^{\frac{1}{2}} \\ &\leq e^{-\frac{1}{2}h(\gamma, T)T} W_2(p_{T, \phi_0}, p_T) + \frac{\epsilon_{\text{DM}}}{\sqrt{2\delta h(\gamma, T)}} (1 - e^{-h(\gamma, T)T})^{\frac{1}{2}}. \end{aligned} \quad (11)$$

Here, the last inequality is from a simple inequality  $\sqrt{a+b} \leq \sqrt{a} + \sqrt{b}$  for nonnegative  $a$  and  $b$ .

By combining inequalities (5), (6), and (11), we obtain

$$\begin{aligned} W_2(p_{0, \theta}, p_{\text{data}}) &\leq e^{-\frac{T}{2}} \left( \mathbb{E}_{p_{\text{data}}(\mathbf{x}_0)} \|\mathbf{x}_0\|_2^2 \right)^{\frac{1}{2}} \Lambda + \Lambda W_2(p_T, p_{T, \phi_0}) \\ &\quad + \mathcal{L}_{\text{PaGoDA}}(\theta; \phi_0) + \left[ \mathbb{E}_{p_{\text{data}}(\mathbf{x}) p_{\phi_0}(\mathbf{z}|\mathbf{x})} \|\mathbf{x} - G^{T \rightarrow 0}(\mathbf{z})\|_2^2 \right]^{\frac{1}{2}} \\ &\quad + e^{-\frac{1}{2}h(\gamma, T)T} W_2(p_T, p_{T, \phi_0}) + \frac{\epsilon_{\text{DM}}}{\sqrt{2\delta h(\gamma, T)}} (1 - e^{-h(\gamma, T)T})^{\frac{1}{2}} \\ &= \mathcal{L}_{\text{rec}}(\theta; \phi_0) + \left[ \mathbb{E}_{p_{\text{data}}(\mathbf{x}) p_{\phi_0}(\mathbf{z}|\mathbf{x})} \|\mathbf{x} - G^{T \rightarrow 0}(\mathbf{z})\|_2^2 \right]^{\frac{1}{2}} \\ &\quad + (\Lambda + e^{-\frac{1}{2}h(\gamma, T)T}) W_2(p_T, p_{T, \phi_0}) \\ &\quad + \frac{\epsilon_{\text{DM}}}{\sqrt{2\delta h(\gamma, T)}} (1 - e^{-h(\gamma, T)T})^{\frac{1}{2}} + e^{-\frac{T}{2}} m\Lambda. \end{aligned}$$

This shows the first inequality in Theorem B.1.

Now, we show the second inequality in the statement of Theorem B.1. First, we establish an upper bound for  $\left[ \mathbb{E}_{p_{\text{data}}(\mathbf{x}) p_{\phi_0}(\mathbf{z}|\mathbf{x})} \|\mathbf{x} - G^{T \rightarrow 0}(\mathbf{z})\|_2^2 \right]^{\frac{1}{2}}$  in terms of  $\epsilon_{\text{DM}}$ . Let  $G_{\phi_0}^{0 \rightarrow T}$  denote the transition map defined by the empirical PF-ODE defined by the teacher  $p_{\phi_0}(\mathbf{x}|\mathbf{z})$ , and  $G^{0 \rightarrow T}$  denote the ground truth transition map defined by the PF-ODE from 0 to  $T$ . Then we have  $\mathbf{x} = G^{T \rightarrow 0}(G^{0 \rightarrow T}(\mathbf{x}))$  for all  $\mathbf{x} \in \text{supp}(p_{\text{data}})$ , and

$$\begin{aligned} \left[ \mathbb{E}_{p_{\text{data}}(\mathbf{x}) p_{\phi_0}(\mathbf{z}|\mathbf{x})} \|\mathbf{x} - G^{T \rightarrow 0}(\mathbf{z})\|_2^2 \right]^{1/2} &= \left[ \mathbb{E}_{p_{\text{data}}(\mathbf{x})} \|G^{T \rightarrow 0}(G^{0 \rightarrow T}(\mathbf{x})) - G^{T \rightarrow 0}(G_{\phi_0}^{0 \rightarrow T}(\mathbf{x}))\|_2^2 \right]^{1/2} \\ &\leq \Lambda \left[ \mathbb{E}_{p_{\text{data}}(\mathbf{x})} \|G^{0 \rightarrow T}(\mathbf{x}) - G_{\phi_0}^{0 \rightarrow T}(\mathbf{x})\|_2^2 \right]^{1/2}. \end{aligned} \quad (12)$$

Here, we utilize the assumption that Assumption I-1 (iii) also holds for  $G^{T \rightarrow 0}$ .

Consider the following two forward-time PF-ODEs on the interval  $[0, T]$ , both starting from  $\mathbf{x}_0 \sim p_{\text{data}}$ :

$$\frac{d\mathbf{x}_t}{dt} = -\mathbf{x}_t - \nabla \log p_t(\mathbf{x}_t), \quad \frac{d\mathbf{x}_{t, \phi_0}}{dt} = -\mathbf{x}_{t, \phi_0} - \mathbf{s}_{\phi_0}(\mathbf{x}_{t, \phi_0}, t).$$

By subtracting them and integrating from 0 to  $t$ , we obtain

$$\|\mathbf{x}_t - \mathbf{x}_{t, \phi_0}\|_2 \leq \underbrace{\mathbf{x}_0 - \mathbf{x}_{0, \phi_0}}_0 + \int_0^t \left\| (\mathbf{x}_\tau - \mathbf{x}_{\tau, \phi_0}) + (\nabla \log p_\tau(\mathbf{x}_\tau) - \mathbf{s}_{\phi_0}(\mathbf{x}_{\tau, \phi_0}, \tau)) \right\|_2 dt$$



$$\leq \int_0^t \|\mathbf{x}_\tau - \mathbf{x}_{\tau, \phi_0}\|_2 d\tau + \epsilon_{\text{DM}} T.$$

By applying Grönwall's inequality,

$$\|\mathbf{x}_t - \mathbf{x}_{t, \phi_0}\|_2 \leq T e^T \epsilon_{\text{DM}}. \quad (13)$$

Combining the above inequality with inequality (12), it implies

$$\left[ \mathbb{E}_{p_{\text{data}(\mathbf{x})} p_{\phi_0}(\mathbf{z}|\mathbf{x})} \|\mathbf{x} - G^{T \rightarrow 0}(\mathbf{z})\|_2^2 \right]^{1/2} \leq \Lambda T e^T \epsilon_{\text{DM}}. \quad (14)$$

Next, we derive an upper bound for  $W_2(p_T, \phi_0, p_T)$  related to  $\epsilon_{\text{DM}}$ . Let  $\pi(\hat{\mathbf{z}}, \mathbf{z})$  be a coupling between  $\hat{\mathbf{z}} \sim p_T, \phi_0 = G_{\phi_0}^{0 \rightarrow T} \# p_{\text{data}}$  and  $\mathbf{z} \sim p_T = G^{0 \rightarrow T} \# p_{\text{data}}$ .

$$W_2^2(p_T, \phi_0, p_T) = W_2^2(G_{\phi_0}^{0 \rightarrow T} \# p_{\text{data}}, G^{0 \rightarrow T} \# p_{\text{data}}) \leq \mathbb{E}_{\pi(\hat{\mathbf{z}}, \mathbf{z})} \|\hat{\mathbf{z}} - \mathbf{z}\|_2^2 \leq (T e^T \epsilon_{\text{DM}})^2, \quad (15)$$

where the last inequality is derived from the inequality (13).

Therefore, with the first conclusion of Theorem B.1 and inequalities (14) and (15), we derive

$$W_2(p_{\theta}, \phi_0, p_{\text{data}}) \lesssim \mathcal{L}_{\text{rec}}(\theta; \phi_0) + \epsilon_{\text{DM}} + e^{-\frac{T}{2}} m \Lambda.$$

■

The proof can be easily extended in two directions: (1) a more general (VP)-SDE:

$$d\mathbf{x}_t = -f(t)\mathbf{x}_t dt + g(t) d\mathbf{w}_t$$

with  $\|f\|_{L^\infty(t; [0, T])}, \|g\|_{L^\infty(t; [0, T])} < \infty$ , and (2) truncation at the least time  $t = \delta$  (instead of  $t = 0$ ), with an additional argument based on [72]

$$\begin{aligned} W_2(p_\delta, p_{\text{data}}) &\leq \left( \mathbb{E}_{p_{\text{data}}(\mathbf{x}_0)} \mathbb{E}_{p_{\text{prior}}(\boldsymbol{\xi})} \left\| (1 - e^{-\delta})\mathbf{x}_0 + \sqrt{1 - e^{-2\delta}}\boldsymbol{\xi} \right\|_2^2 \right)^{\frac{1}{2}} \\ &\leq \left( (1 - e^{-\delta})^2 m^2 + (1 - e^{-2\delta}) D \right)^{\frac{1}{2}} \\ &\lesssim (\sqrt{D} \vee m) \sqrt{\delta}, \end{aligned}$$

where  $p_\delta = G^{T \rightarrow \delta} \# p_{\text{prior}}$ .

### B.1.3 $W_1$ Bound with PaGoDA's Reconstruction Loss

**Assumption II-1.** (i)  $m := \mathbb{E}_{p_{\text{data}}(\mathbf{x})} \|\mathbf{x}\|_2 < \infty$ ;

(ii) There is a  $\epsilon_{\text{DSM}} > 0$  so that  $\sup_{\mathbf{x}, t} \|\mathbf{s}_\phi(\mathbf{x}, t) - \nabla \log p_t(\mathbf{x})\|_2^2 \leq \epsilon_{\text{DSM}}^2$ ;

(iii)  $G_\theta^{T \rightarrow 0}$  is Lipschitz in  $\mathbf{x}$ :

$$\Lambda := \sup_{\mathbf{x} \neq \mathbf{y}} \frac{\|G_\theta^{T \rightarrow 0}(\mathbf{x}) - G_\theta^{T \rightarrow 0}(\mathbf{y})\|_2}{\|\mathbf{x} - \mathbf{y}\|_2} < \infty,$$

for all  $\theta$  and  $T$ .

(iv)  $\nabla \log p_t(\cdot)$  is Lipschitz in  $\mathbf{x}$  with integrable Lipschitz constant:

$$\Lambda_s(t) := \sup_{\mathbf{x} \neq \mathbf{y}} \frac{\|\nabla \log p_t(\mathbf{x}) - \nabla \log p_t(\mathbf{y})\|_2}{\|\mathbf{x} - \mathbf{y}\|_2} < \infty,$$

and  $\Lambda_s$  is an  $L^1$ -integrable function on  $(0, \infty)$ .

In the following proposition, we prove a variant of Theorem B.1 which does not assume log-concavity of the data density (i.e., Assumption I-1 (iv)).

**Theorem B.3** (Variant of Theorem B.1). Assume that Assumption II-1 holds. Let  $\nu$  be either the oracle data distribution  $p_{data}$  or an empirical distribution  $\hat{p}_{data,N} := \frac{1}{N} \sum_{i=1}^N \delta_{\mathbf{x}_i}$ , where  $\mathbf{x}_i \sim p_{data}$  for  $i = 1, \dots, N$ . Let the PaGoDA's reconstruction loss starting from  $\nu$  be defined as

$$\mathcal{L}_{rec}(\boldsymbol{\theta}_\nu; \boldsymbol{\phi}_0) := \mathbb{E}_{\nu(\mathbf{x})p_{\phi_0}(\mathbf{z}|\mathbf{x})} [\|\mathbf{x} - G_{\boldsymbol{\theta}_\nu}^{T \rightarrow 0}(\mathbf{z})\|_2].$$

Then we have

$$\begin{aligned} W_1(p_{0,\boldsymbol{\theta}}, \nu) &\leq \mathcal{L}_{rec}(\boldsymbol{\theta}_\nu; \boldsymbol{\phi}_0) + \mathbb{E}_{\nu(\mathbf{x})p_{\phi_0}(\mathbf{z}|\mathbf{x})} [\|\mathbf{x} - G^{T \rightarrow 0}(\mathbf{z})\|_2] + C_T T \epsilon_{DM} \\ &\quad + (C_T + \Lambda) W_1(p_T, \phi_0, p_T) + e^{-T} (\mathbb{E}_{p_{data}(\mathbf{x}_0)} \|\mathbf{x}_0\|_2) \Lambda \end{aligned}$$

In particular, if we assume Assumption I-1 (iii) holds also for  $G^{T \rightarrow 0}$ , then for  $T = \mathcal{O}\left(\log\left(\frac{m\Lambda}{\epsilon_{DM}}\right)^2\right)$  is sufficiently large, we have

$$W_1(p_{0,\boldsymbol{\theta}}, p_{data}) \lesssim \mathcal{L}_{rec}(\boldsymbol{\theta}; \boldsymbol{\phi}_0) + \epsilon_{DM}.$$

Here, we use  $\lesssim$  to absorb the dependence on the constants  $T$  and  $\gamma$  into the inequality.

**Proof of Theorem B.3.** Define  $p_{T,\phi_0} := G_{\phi_0}^{0 \rightarrow T} \# \nu$ , and  $p_{0,\phi_0} := G^{T \rightarrow 0} \# p_{T,\phi_0}$ . From the triangle inequality, we have

$$W_1(p_{0,\boldsymbol{\theta}}, \nu) \leq \underbrace{W_1(p_{0,\boldsymbol{\theta}}, p_{0,\phi_0})}_{(A)} + \underbrace{W_1(p_{0,\phi_0}, \nu)}_{(B)}.$$

For (A), by following the similar argument as in Theorem B.1, we can obtain

$$(A) \leq e^{-T} (\mathbb{E}_{p_{data}(\mathbf{x}_0)} \|\mathbf{x}_0\|_2) \Lambda + \Lambda W_1(p_T, p_T, \phi_0) + \mathcal{L}_{PaGoDA}(\boldsymbol{\theta}_\nu; \boldsymbol{\phi}_0) + \mathbb{E}_{\nu(\mathbf{x})p_{\phi_0}(\mathbf{z}|\mathbf{x})} [\|\mathbf{x} - G^{T \rightarrow 0}(\mathbf{z})\|_2] \quad (16)$$

For (B), by subtracting the following equations and integrating over  $t$  from 0 to  $T$ ,

$$\begin{cases} \frac{d\hat{\mathbf{z}}_{t,\phi_0}}{dt} = \hat{\mathbf{z}}_{t,\phi_0} + \mathbf{s}_{\phi_0}(\hat{\mathbf{z}}_{t,\phi_0}, T-t), & \hat{\mathbf{z}}_{0,\phi_0} \sim p_{T,\phi_0} \\ \frac{d\hat{\mathbf{z}}_t}{dt} = \hat{\mathbf{z}}_t + \nabla \log p_{T-t}(\hat{\mathbf{z}}_t), & \hat{\mathbf{z}}_0 \sim p_T, \end{cases}$$

we will obtain

$$\hat{\mathbf{z}}_{T,\phi_0} - \hat{\mathbf{z}}_T = (\hat{\mathbf{z}}_{0,\phi_0} - \hat{\mathbf{z}}_0) + \int_0^T (\mathbf{s}_{\phi_0}(\hat{\mathbf{z}}_{t,\phi_0}, T-t) - \nabla \log p_{T-t}(\hat{\mathbf{z}}_t)) du.$$

Now let  $u(t) := \mathbb{E} \|\hat{\mathbf{z}}_{t,\phi_0} - \hat{\mathbf{z}}_t\|_2$ . Then

$$\begin{aligned} u(t) &\leq u(0) + \mathbb{E} \int_0^t \|\mathbf{s}_{\phi_0}(\hat{\mathbf{z}}_{\tau,\phi_0}, T-\tau) - \nabla \log p_{T-\tau}(\hat{\mathbf{z}}_\tau)\|_2 d\tau \\ &\leq u(0) + \int_0^T \mathbb{E} \|\mathbf{s}_{\phi_0}(\hat{\mathbf{z}}_{\tau,\phi_0}, T-\tau) - \nabla \log p_{T-\tau}(\hat{\mathbf{z}}_{\tau,\phi_0})\|_2 d\tau \\ &\quad + \int_0^t \mathbb{E} \|\nabla \log p_{T-\tau}(\hat{\mathbf{z}}_{\tau,\phi_0}) - \nabla \log p_{T-\tau}(\hat{\mathbf{z}}_\tau)\|_2 d\tau \\ &\leq u(0) + T \epsilon_{DM} + \int_0^t \Lambda_s(\tau) u(\tau) d\tau, \end{aligned}$$

where  $\Lambda_s(t)$  is the Lipschitz constant of  $\nabla \log p_t(\cdot)$  in  $\mathbf{x}$ . By applying integral form of Grönwall's inequality, we get

$$(B) \leq \mathbb{E} \|\hat{\mathbf{z}}_{T,\phi_0} - \hat{\mathbf{z}}_T\|_2 \leq C_T \mathbb{E} \|\hat{\mathbf{z}}_{0,\phi_0} - \hat{\mathbf{z}}_0\|_2 + C_T T \epsilon_{DM} = C_T W_1(p_T, \phi_0, p_T) + C_T T \epsilon_{DM}. \quad (17)$$

where  $C_T := \exp\left(\int_0^T \Lambda_s(t) dt\right)$  and the last equality follows from choosing a coupling of  $\hat{\mathbf{z}}_{0,\phi_0} \sim p_{T,\phi_0}$  and  $\hat{\mathbf{z}}_0 \sim p_T$  so that  $W_1(p_T, \phi_0, p_T) = \mathbb{E} \|\hat{\mathbf{z}}_{0,\phi_0} - \hat{\mathbf{z}}_0\|_2$ .

By combining inequalities (16) and (17), we obtain

$$\begin{aligned} W_1(p_{0,\boldsymbol{\theta}}, \nu) &\leq \mathcal{L}_{rec}(\boldsymbol{\theta}_\nu; \boldsymbol{\phi}_0) + \mathbb{E}_{\nu(\mathbf{x})p_{\phi_0}(\mathbf{z}|\mathbf{x})} [\|\mathbf{x} - G^{T \rightarrow 0}(\mathbf{z})\|_2] + C_T T \epsilon_{DM} \\ &\quad + (C_T + \Lambda) W_1(p_T, \phi_0, p_T) + e^{-T} (\mathbb{E}_{p_{data}(\mathbf{x}_0)} \|\mathbf{x}_0\|_2) \Lambda. \end{aligned}$$

A similar argument to Theorem B.1 can be applied to obtain the second inequality in the statement of Theorem B.3.  $\blacksquare$

## B.2 Optimality analysis

In this section, we compare the optimality of the learned distributions resulting from PaGoDA’s training and distillation-based training loss, incorporating GAN [8, 18].

**PaGoDA’s Loss** We recall PaGoDA’s training objective  $\mathcal{L}_{\text{PaGoDA}}$

$$\mathcal{L}_{\text{PaGoDA}}(G_\theta, D_\psi) = \mathcal{L}_{\text{rec}}(G_\theta) + \lambda \mathcal{L}_{\text{adv}}(G_\theta, D_\psi)$$

leverages the reconstruction loss

$$\mathcal{L}_{\text{rec}}(G_\theta) = \mathbb{E}_{p_{\text{data}}(\mathbf{x})} \left[ \|\mathbf{x} - G_\theta(E(\mathbf{x}))\|_2^2 \right],$$

and adversarial loss

$$\mathcal{L}_{\text{adv}}(G_\theta, D_\psi) = \mathbb{E}_{p_{\text{data}}(\mathbf{x})} [\log D_\psi(\mathbf{x})] + \mathbb{E}_{p_{\text{prior}}(\mathbf{z})} \left[ \log \left( 1 - D_\psi(G_\theta(\mathbf{z})) \right) \right].$$

**Knowledge Distillation Loss** In the realm of knowledge distillation (KD) methods for DMs, approaches like *local consistency* [7], *global consistency* [18], or *soft consistency* [8] are utilized to learn the noise-to-data trajectory of the teacher DM. Let us consider the global consistency loss as a case study (similar arguments can apply to other distillation objectives), where the teacher’s trajectory is obtained by solving its empirical PF-ODE from  $T$  to 0. The long jump along the trajectory is represented as  $G_{\text{teacher}}^{T \rightarrow 0}(\mathbf{z})$ , where  $\mathbf{z}$  denotes the initial point (noise),  $T$  signifies the initial time, and 0 denotes the final time. The output of  $G_{\text{teacher}}^{T \rightarrow 0}$  corresponds to the estimation of clean data, starting from  $\mathbf{z}$ .

$$\mathcal{L}_{\text{KD}}(G_\theta) := \mathbb{E}_{p_{\text{prior}}(\mathbf{z})} \left[ \left\| G_{\text{teacher}}^{T \rightarrow 0}(\mathbf{z}) - G_\theta(\mathbf{z}) \right\|_2^2 \right].$$

In this context, we abuse the notation  $G_\theta(\mathbf{z})$  to denote the generator for KD.

The training of KD can also incorporate adversarial loss for enhanced performance [8, 32]. We represent the combined loss as:

$$\mathcal{L}_{\text{KD+GAN}}(G_\theta, D_\psi) := \mathcal{L}_{\text{KD}}(G_\theta) + \mathcal{L}_{\text{adv}}(G_\theta, D_\psi).$$

**Theorem B.4.** *Let  $p_{\phi_0}$  be the density determined the teacher DM. Suppose that GAN admits an optimal discriminator  $D^*$ .*

- *In PaGoDA, assume that the network parametrized generator class  $\{G_\theta\}$  is expressive enough so that it can simultaneously optimize both  $\mathcal{L}_{\text{rec}}(G_\theta)$  and  $\mathcal{L}_{\text{adv}}(G_\theta; D^*)$  with a same minimizer. Namely,  $\arg \min_{\theta} \{\mathcal{L}_{\text{rec}}(G_\theta)\} \cap \arg \min_{\theta} \{\mathcal{L}_{\text{adv}}(G_\theta; D^*)\} \neq \emptyset$ . Then*

$$p_{\theta^*, \text{PaGoDA}} := G_{\theta^*, \text{PaGoDA}} \# p_{\text{prior}} = p_{\text{data}}.$$

- *In contrast, suppose that  $p_{\phi_0} \neq p_{\text{data}}$ , then under similar conditions for KD+GAN where  $\arg \min_{\theta} \{\mathcal{L}_{\text{KD}}(G_\theta)\} \cap \arg \min_{\theta} \{\mathcal{L}_{\text{adv}}(G_\theta; D^*)\} \neq \emptyset$ , there is no minimizer  $\theta^*$  so that  $p_{\theta^*, \text{KD+GAN}} := G_{\theta^*, \text{KD+GAN}} \# p_{\text{prior}} = p_{\text{data}}$ .*

The first part of the proof of the theorem follows from the following Lemma.

**Lemma B.5.** *If  $\arg \min_{\theta} \{f(\theta)\} \cap \arg \min_{\theta} \{g(\theta)\} \neq \emptyset$ , then  $\arg \min_{\theta} \{f(\theta) + g(\theta)\} = \arg \min_{\theta} \{f(\theta)\} \cap \arg \min_{\theta} \{g(\theta)\}$ .*

*Proof.* First, we prove the relationship  $\arg \min_{\theta} \{f(\theta) + g(\theta)\} \supseteq \arg \min_{\theta} \{f(\theta)\} \cap \arg \min_{\theta} \{g(\theta)\}$ . Indeed, it holds without additional assumption. Suppose that  $\theta^* \in \arg \min_{\theta} \{f(\theta)\} \cap \arg \min_{\theta} \{g(\theta)\}$ . Then for any  $\theta$ , we have  $f(\theta) \geq f(\theta^*)$  and  $g(\theta) \geq g(\theta^*)$ , which implies  $f(\theta) + g(\theta) \geq f(\theta^*) + g(\theta^*)$ . That is,  $\theta^* \in \arg \min_{\theta} \{f(\theta) + g(\theta)\}$ .

On the other hand, suppose that  $\theta^* \in \arg \min_{\theta} \{f(\theta) + g(\theta)\}$ . We want to prove that  $\theta^* \in \arg \min_{\theta} \{f(\theta)\} \cap \arg \min_{\theta} \{g(\theta)\}$ . Let  $\theta_{\bar{n}}^* \in \arg \min_{\theta} \{f(\theta)\} \cap \arg \min_{\theta} \{g(\theta)\}$ , where we notice that the existence of  $\theta_{\bar{n}}^*$  is guaranteed by the assumption. In particular, we have  $f(\theta^*) \geq f(\theta_{\bar{n}}^*)$  and  $g(\theta^*) \geq g(\theta_{\bar{n}}^*)$ . Then for any  $\theta$ , we have

$$\min_{\theta} \{f(\theta) + g(\theta)\} = f(\theta^*) + g(\theta^*) \geq f(\theta_{\bar{n}}^*) + g(\theta_{\bar{n}}^*) \geq \min_{\theta} \{f(\theta) + g(\theta)\}.$$

Thus,  $\min_{\theta} \{f(\theta) + g(\theta)\} = f(\theta^*) + g(\theta^*) = f(\theta_{\bar{\cdot}}^*) + g(\theta_{\bar{\cdot}}^*)$  and

$$[f(\theta^*) - f(\theta_{\bar{\cdot}}^*)] + [g(\theta^*) - g(\theta_{\bar{\cdot}}^*)] = 0.$$

This implies  $f(\theta^*) = f(\theta_{\bar{\cdot}}^*) = \min_{\theta} \{f(\theta)\}$  and  $g(\theta^*) = g(\theta_{\bar{\cdot}}^*) = \min_{\theta} \{g(\theta)\}$ , as the individual terms are nonnegative. Therefore,  $\theta^* \in \arg \min_{\theta} \{f(\theta)\} \cap \arg \min_{\theta} \{g(\theta)\}$ , which concludes the proof.  $\square$

**Proof of Theorem B.4.** With the lemma above, let  $\theta^* \in \arg \min_{\theta} \mathcal{L}_{\text{PaGoDA}}(G_{\theta}, D^*)$ . Consequently,  $\theta^*$  should also simultaneously minimize both  $\mathcal{L}_{\text{rec}}$  and  $\mathcal{L}_{\text{adv}}$ . Minimizing  $\mathcal{L}_{\text{rec}}$  implies that  $p_{\theta^*, \text{PaGoDA}} = G_{\theta^*, \text{PaGoDA}} \# p_{T, \phi_0}$ , where  $p_{T, \phi_0}$  represents the density derived from solving the teacher’s empirical PF-ODE forward, starting from  $p_{\text{data}}$ . On the other hand, optimizing  $\mathcal{L}_{\text{adv}}$  implies that  $p_{\theta^*, \text{PaGoDA}} = p_{\text{data}}$  by applying Theorem 1 in [5]. This establishes the first part of the theorem.

In the second part, suppose on the contrary that there is a minimizer  $\theta^*$  of  $\mathcal{L}_{\text{KD+GAN}}$  such that  $p_{\theta^*, \text{KD+GAN}} = p_{\text{data}}$ . Again, by applying the above lemma, we infer that  $\theta^*$  should also minimize  $\mathcal{L}_{\text{KD}}$  (and  $\mathcal{L}_{\text{adv}}$ ). This implies that  $p_{\theta^*, \text{KD+GAN}} = p_{\phi_0}$ . However, this contradicts our assumption that  $p_{\text{data}} \neq p_{\phi_0}$ . Thus, such a minizer does not exist and the second part of the theorem is proven.  $\blacksquare$

We remark that (1) optimality of  $\mathcal{L}_{\text{GAN}}(\theta)$  may not be unique in  $\theta$ , and that (2) the first part of the theorem can be directly extended to scenarios involving downsampling in the encoder.

### B.3 Stability Analysis

#### B.3.1 Preliminaries of Dynamical System

To study its convergence and stability, we first introduce the prerequisites for Lyapunov stability [74, 75] in a general setup. Let  $\mathcal{F}: \Xi \rightarrow \Xi$  be a continuously differentiable operator (that is,  $\mathcal{C}^1$  operator), where  $\Omega \subset \mathbb{R}^N$ . We consider the discrete iteration dynamical system defined by

$$\xi_{k+1} = \mathcal{F}(\xi_k) \quad \text{with } \xi_0 \in \Omega.$$

Namely,  $\xi_{k+1} = \mathcal{F}^{(k)}(\xi_0) := \underbrace{\mathcal{F} \circ \dots \circ \mathcal{F}}_{k\text{-copies}}(\xi_0)$ . A point  $\xi^* \in \Omega$  is called a *fixed point* or *equilibrium*

(we use the terms interchangeably) of  $\mathcal{F}$  if  $\xi^* = \mathcal{F}(\xi^*)$ . The stability and convergence analysis focuses on how the dynamical system  $\mathcal{F}^{(k)}(\xi_0)$  approaches a fixed point as iterations  $k$  are sufficiently large.

**Definition B.1.** (Stability [75]) Let  $\xi^*$  be an equilibrium of the  $\mathcal{C}^1$  operator  $\mathcal{F}: \Omega \rightarrow \Omega$ . The equilibrium  $\xi^*$  is said to be

- *stable* if for every  $\epsilon > 0$  there is a  $\delta > 0$  so that whenever  $\|\xi - \xi^*\|_2 < \delta$ , we have  $\|\mathcal{F}^{(k)}(\xi) - \xi^*\|_2 < \epsilon$  for all  $k \in \mathbb{N} \cup \{0\}$ .
- *asymptotically stable* if  $\xi^*$  is stable, and there is a  $\delta > 0$  so that whenever  $\|\xi - \xi^*\|_2 < \delta$ , we have  $\lim_{k \rightarrow \infty} \|\mathcal{F}^{(k)}(\xi) - \xi^*\|_2 = 0$ .
- *exponentially stable* if  $\xi^*$  is asymptotically stable, and there is a  $\delta > 0$  and  $\alpha, \beta > 0$  so that whenever  $\|\xi - \xi^*\|_2 < \delta$ , we have  $\|\mathcal{F}^{(k)}(\xi) - \xi^*\|_2 \leq \alpha \|\xi - \xi^*\|_2 e^{-\beta k}$  for all  $k \in \mathbb{N} \cup \{0\}$ . The largest  $\beta > 0$  that satisfies the inequality for exponential stability is referred to as the *rate of convergence*.

Let  $\Gamma$  be a subset of the set of all equilibria. We say the dynamical system  $\mathcal{F}^{(k)}$  *locally converges* on  $\Gamma$  if  $\mathcal{F}^{(k)}$  is exponentially stable at any point in  $\Gamma$ .

The intuitions of the above stability notions are

- A *stable* equilibrium indicates that if an initialization is within some  $\delta$ -neighborhood of the equilibrium, the iterations starting from that initialization will always remain within an  $\epsilon$ -neighborhood of the equilibrium, for any arbitrarily chosen  $\epsilon$ .

- An *asymptotically stable* equilibrium indicates that iterations starting near the equilibrium not only remain close but ultimately converge to the equilibrium.
- An *asymptotically stable* equilibrium indicates that the iterations not only converge but do so at a rate no slower than the rate  $e^{-\beta k}$  with respect to iteration step  $k$ .

Analyzing the eigenvalues of the Jacobian  $\nabla_{\xi} \mathcal{F}(\xi^*)$  of the operator  $\mathcal{F}$  at an equilibrium  $\xi^*$  is a crucial tool for studying stability. In principle [74, 75], if we can ensure that the Jacobian of  $\mathcal{F}$  at some equilibrium has only eigenvalues with strictly negative real parts, then the dynamical system  $\mathcal{F}^{(k)}$  is asymptotically stable at that equilibrium. In particular, we refer to a matrix as a *Hurwitz matrix* if all its eigenvalues have strictly negative real parts.

In the following lemma, we present a necessary condition to ensure that a special class of matrices will be Hurwitz.

**Lemma B.6.** (Necessary condition for a Hurwitz matrix [27]) Consider the following matrix  $\mathcal{J} \in \mathbb{R}^{(N+M) \times (N+M)}$  with  $P \in \mathbb{R}^{N \times N}$ ,  $Q \in \mathbb{R}^{M \times M}$ , and  $B \in \mathbb{R}^{M \times N}$ .

$$\mathcal{J} = \begin{bmatrix} P & -B^T \\ B & Q \end{bmatrix}.$$

Suppose that  $B$  is full rank. Then all eigenvalues of  $\mathcal{J}$  have negative real part, if either (1)  $P$  is negative definite and  $Q$  is negative semi-definite, or (2)  $P$  is negative semi-definite and  $Q$  is negative definite.

### B.3.2 Preliminaries for Analysis of PaGoDA Training

We consider PaGoDA’s training, integrating reconstruction and adversarial losses with a weight  $\eta > 0$ .

$$\mathcal{L}(\theta, \psi) := \mathbb{E}_{p_{\text{data}}(\mathbf{x})} [\eta \|\mathbf{x} - G_{\theta}(E(\mathbf{x}))\|_2^2 + f(D_{\psi}(\mathbf{x}))] + \mathbb{E}_{p_{G_{\theta}}(\mathbf{x})} [f(-D_{\psi}(\mathbf{x}))] \quad (18)$$

$$= \mathbb{E}_{p_{\text{data}}(\mathbf{x})} [\eta \|\mathbf{x} - G_{\theta}(E(\mathbf{x}))\|_2^2 + f(D_{\psi}(\mathbf{x}))] + \mathbb{E}_{p_{\text{prior}}(\mathbf{z})} [f(-D_{\psi}(G_{\theta}(\mathbf{z})))] \quad (19)$$

Here,  $f: \mathbb{R} \rightarrow \mathbb{R}$  is a continuous differentiable function. In the vanilla GAN [5], the  $f$ -function is taken as  $f(u) := -\log(1 + \exp(-u))$ , where  $f'(u) = \exp(-u)/(1 + \exp(-u)) > 0$  and  $f''(u) = -\exp(-u)/(1 + \exp(-u)) < 0$  for all  $u \in \mathbb{R}$ . We maintain the generality of  $f$  and will prove the training stability of PaGoDA across a wide class of  $f$ .

The velocity field  $\mathbf{v}(\theta, \psi)$  corresponding to the gradient descent update is

$$\mathbf{v}(\theta, \psi) := \begin{bmatrix} -\nabla_{\theta} \mathcal{L}(\theta, \psi) \\ \nabla_{\psi} \mathcal{L}(\theta, \psi) \end{bmatrix}.$$

Gradient descent is a special case of fixed-point iteration. Now, we specify the operator  $\mathcal{F}$  as an alternative gradient descent operator. That is, we consider  $\mathcal{F}_h := \mathcal{F}_{D,h} \circ \mathcal{F}_{G,h}$  with a learning rate  $h > 0$ . Here,

$$\mathcal{F}_{G,h}(\theta, \psi) := \begin{bmatrix} \theta - h \nabla_{\theta} \mathcal{L}(\theta, \psi) \\ \psi \end{bmatrix} \quad \text{and} \quad \mathcal{F}_{D,h}(\theta, \psi) := \begin{bmatrix} \theta \\ \psi + h \nabla_{\psi} \mathcal{L}(\theta, \psi) \end{bmatrix}.$$

A point  $(\theta^*, \psi^*)$  is called an *equilibrium* of the system defined by  $\mathbf{v}$  if  $\mathbf{v}(\theta^*, \psi^*) = 0$  (equivalently,  $\mathcal{F}_h(\theta^*, \psi^*) = 0$ ). We can analyze the learning dynamic via the Jacobian matrix of  $\mathbf{v}(\theta, \psi)$  which is defined as the following:

$$\mathcal{J}(\theta, \psi) := \begin{bmatrix} -\nabla_{\theta}^2 \mathcal{L}(\theta, \psi) & -\nabla_{\theta, \psi}^2 \mathcal{L}(\theta, \psi) \\ \nabla_{\theta, \psi}^2 \mathcal{L}(\theta, \psi) & \nabla_{\psi}^2 \mathcal{L}(\theta, \psi) \end{bmatrix}.$$

The following proposition relates Lemma B.8 to the stability of the gradient descent operator  $\mathcal{F}_h$ , serving as the main tool to prove the training stability of PaGoDA in Theorem B.9.

**Lemma B.7.** (Locally stable on manifold – modification of [27]) Suppose that the gradient descent operator  $\mathcal{F}_h = \mathcal{F}_h(\mathbf{v}, \omega)$  is a  $\mathcal{C}^1$  mapping. Let  $(\mathbf{v}^*, \omega^*)$  be an equilibrium (fixed point) of  $\mathcal{F}_h$ . Assume that there is a neighborhood  $\Omega$  of  $\omega^*$  so that  $\mathcal{F}_h$  admits equilibrium on  $\{\mathbf{v}^*\} \times \Omega$ :

$$\mathcal{F}_h(\mathbf{v}^*, \omega) = (\mathbf{v}^*, \omega) \quad \text{for all } \omega \in \Omega.$$

If all the eigenvalues of  $\mathcal{J} := \nabla_{\mathbf{v}} \mathcal{F}_h(\mathbf{v}^*, \boldsymbol{\omega}^*)$  have negative real parts, then for a sufficiently small learning rate  $h$ , the gradient descent iteration defined by  $\mathcal{F}_h$  locally converges on  $\Gamma := \{(\mathbf{v}^*, \boldsymbol{\omega}) \mid \boldsymbol{\omega} \in \Omega\}$  with a rate of convergence  $|\lambda_{\max}|$ . Here,  $\lambda_{\max}$  denotes the eigenvalue of  $\mathcal{J}$  with the largest absolute value.

**Proof of Lemma B.7.** This proposition is followed by Lemma A.5. and Theorem A.3. of [27]. ■

### B.3.3 PaGoDA's Training is Stable

Proving PaGoDA's stability involves two steps: First, derive the components of First, deriving the components of  $\mathcal{J}(\boldsymbol{\theta}^*, \boldsymbol{\psi}^*)$ . Second, verify that these components satisfy Lemma B.6. After these, we can apply Lemma B.7 to conclude PaGoDA's training stability whenever the learning rate  $h > 0$  is sufficiently small.

**Assumption III-1.** (i)  $E$  is not an identity map.

(ii) At  $\boldsymbol{\theta}^*$ ,  $p_{\boldsymbol{\theta}^*} = p_{\text{data}}$ , and  $\mathbf{x} = G_{\boldsymbol{\theta}^*}(E(\mathbf{x}))$  for a.e.  $\mathbf{x} \in \text{supp}(p_{\text{data}})$ .

(iii) At  $\boldsymbol{\psi}^*$ ,  $D_{\boldsymbol{\psi}^*}(\mathbf{x}) = 0$  and  $\nabla_{\mathbf{x}} D_{\boldsymbol{\psi}^*}(\mathbf{x}) = 0$  for  $\mathbf{x} \in \text{supp}(p_{\text{data}})$ .

**Lemma B.8.** Suppose that Assumption III-1 holds for an equilibrium  $(\boldsymbol{\theta}^*, \boldsymbol{\psi}^*)$ . Then the Jacobian at the equilibrium can be computed as

$$\mathcal{J}(\boldsymbol{\theta}^*, \boldsymbol{\psi}^*) = \begin{bmatrix} K_{GG} & -K_{DG}^T \\ K_{DG} & K_{DD} \end{bmatrix}.$$

Here, and

$$\begin{aligned} K_{GG} &= -2\eta \mathbb{E}_{p_{\text{data}}(\mathbf{x})} [\nabla_{\boldsymbol{\theta}} G_{\boldsymbol{\theta}^*}(E(\mathbf{x}))^T \cdot \nabla_{\boldsymbol{\theta}} G_{\boldsymbol{\theta}^*}(E(\mathbf{x}))] \\ &\quad + f'(0) \mathbb{E}_{p_{\text{prior}}(\mathbf{z})} [\nabla_{\boldsymbol{\theta}} G_{\boldsymbol{\theta}^*}(\mathbf{z})^T \cdot \nabla_{\mathbf{x}}^2 D_{\boldsymbol{\psi}^*}(G_{\boldsymbol{\theta}^*}(\mathbf{z})) \cdot \nabla_{\boldsymbol{\theta}} G_{\boldsymbol{\theta}^*}(\mathbf{z})]. \\ K_{DG} &= -f'(0) \nabla_{\boldsymbol{\theta}} \mathbb{E}_{p_{G_{\boldsymbol{\theta}}(\mathbf{x})}} [\nabla_{\boldsymbol{\psi}} D_{\boldsymbol{\psi}^*}(\mathbf{x})] \Big|_{\boldsymbol{\theta}=\boldsymbol{\theta}^*} \\ K_{DD} &= 2f''(0) \mathbb{E}_{p_{\text{data}}(\mathbf{x})} [\nabla_{\boldsymbol{\psi}} D_{\boldsymbol{\psi}^*}(\mathbf{x}) \cdot \nabla_{\boldsymbol{\psi}} D_{\boldsymbol{\psi}^*}(\mathbf{x})^T]. \end{aligned}$$

**Proof of Lemma B.8.** We first compute the gradients of  $\mathcal{L}$  in terms of  $\boldsymbol{\theta}$  and  $\boldsymbol{\psi}$ , where we utilize the formulations Eqs. (18) and (19), respectively.

$$\begin{aligned} \nabla_{\boldsymbol{\theta}} \mathcal{L}(\boldsymbol{\theta}, \boldsymbol{\psi}) &= -2\eta \mathbb{E}_{p_{\text{data}}(\mathbf{x})} [\langle \mathbf{x} - G_{\boldsymbol{\theta}}(E(\mathbf{x})), \nabla_{\boldsymbol{\theta}} G_{\boldsymbol{\theta}}(E(\mathbf{x})) \rangle] \\ &\quad - \mathbb{E}_{p_{\text{prior}}(\mathbf{z})} [f'(-D_{\boldsymbol{\psi}}(G_{\boldsymbol{\theta}}(\mathbf{z}))) \cdot \nabla_{\mathbf{x}} D_{\boldsymbol{\psi}}(G_{\boldsymbol{\theta}}(\mathbf{z})) \cdot \nabla_{\boldsymbol{\theta}} G_{\boldsymbol{\theta}}(\mathbf{z})]. \end{aligned} \quad (20)$$

$$\nabla_{\boldsymbol{\psi}} \mathcal{L}(\boldsymbol{\theta}, \boldsymbol{\psi}) = \mathbb{E}_{p_{\text{data}}(\mathbf{x})} [f'(D_{\boldsymbol{\psi}}(\mathbf{x})) \nabla_{\boldsymbol{\psi}} D_{\boldsymbol{\psi}}(\mathbf{x})] - \mathbb{E}_{p_{G_{\boldsymbol{\theta}}(\mathbf{x})}} [f'(-D_{\boldsymbol{\psi}}(\mathbf{x})) \nabla_{\boldsymbol{\psi}} D_{\boldsymbol{\psi}}(\mathbf{x})]. \quad (21)$$

$$\begin{aligned} \nabla_{\boldsymbol{\theta}}^2 \mathcal{L}(\boldsymbol{\theta}, \boldsymbol{\psi}) &= 2\eta \mathbb{E}_{p_{\text{data}}(\mathbf{x})} [\langle \nabla_{\boldsymbol{\theta}} G_{\boldsymbol{\theta}}(E(\mathbf{x})), \nabla_{\boldsymbol{\theta}} G_{\boldsymbol{\theta}}(E(\mathbf{x})) \rangle] - 2\eta \mathbb{E}_{p_{\text{data}}(\mathbf{x})} [\langle \mathbf{x} - G_{\boldsymbol{\theta}}(E(\mathbf{x})), \nabla_{\boldsymbol{\theta}}^2 G_{\boldsymbol{\theta}}(E(\mathbf{x})) \rangle] \\ &\quad + \mathbb{E}_{p_{\text{prior}}(\mathbf{z})} [f''(-D_{\boldsymbol{\psi}}(G_{\boldsymbol{\theta}}(\mathbf{z}))) \cdot \nabla_{\mathbf{x}} D_{\boldsymbol{\psi}}(G_{\boldsymbol{\theta}}(\mathbf{z})) \cdot \nabla_{\boldsymbol{\theta}} G_{\boldsymbol{\theta}}(\mathbf{z}) \cdot \nabla_{\mathbf{x}} D_{\boldsymbol{\psi}}(G_{\boldsymbol{\theta}}(\mathbf{z})) \cdot \nabla_{\boldsymbol{\theta}} G_{\boldsymbol{\theta}}(\mathbf{z})] \\ &\quad - \mathbb{E}_{p_{\text{prior}}(\mathbf{z})} [f'(-D_{\boldsymbol{\psi}}(G_{\boldsymbol{\theta}}(\mathbf{z}))) \cdot \nabla_{\boldsymbol{\theta}} G_{\boldsymbol{\theta}}(\mathbf{z})^T \cdot \nabla_{\mathbf{x}}^2 D_{\boldsymbol{\psi}}(G_{\boldsymbol{\theta}}(\mathbf{z})) \cdot \nabla_{\boldsymbol{\theta}} G_{\boldsymbol{\theta}}(\mathbf{z})] \\ &\quad - \mathbb{E}_{p_{\text{prior}}(\mathbf{z})} [f'(-D_{\boldsymbol{\psi}}(G_{\boldsymbol{\theta}}(\mathbf{z}))) \cdot \nabla_{\mathbf{x}} D_{\boldsymbol{\psi}}(G_{\boldsymbol{\theta}}(\mathbf{z})) \cdot \nabla_{\boldsymbol{\theta}}^2 G_{\boldsymbol{\theta}}(\mathbf{z})]. \end{aligned}$$

According to Assumption III-1 (ii) and (iii), we have

$$\begin{aligned} \nabla_{\boldsymbol{\theta}}^2 \mathcal{L}(\boldsymbol{\theta}^*, \boldsymbol{\psi}^*) &= 2\eta \mathbb{E}_{p_{\text{data}}(\mathbf{x})} [\nabla_{\boldsymbol{\theta}} G_{\boldsymbol{\theta}^*}(E(\mathbf{x}))^T \cdot \nabla_{\boldsymbol{\theta}} G_{\boldsymbol{\theta}^*}(E(\mathbf{x}))] \\ &\quad - f'(0) \mathbb{E}_{p_{\text{prior}}(\mathbf{z})} [\nabla_{\boldsymbol{\theta}} G_{\boldsymbol{\theta}^*}(\mathbf{z})^T \cdot \nabla_{\mathbf{x}}^2 D_{\boldsymbol{\psi}}(G_{\boldsymbol{\theta}^*}(\mathbf{z})) \cdot \nabla_{\boldsymbol{\theta}} G_{\boldsymbol{\theta}^*}(\mathbf{z})]. \end{aligned}$$

Thus, we obtain

$$\begin{aligned} K_{GG} &= -\nabla_{\boldsymbol{\theta}}^2 \mathcal{L}(\boldsymbol{\theta}^*, \boldsymbol{\psi}^*) \\ &= -2\eta \mathbb{E}_{p_{\text{data}}(\mathbf{x})} [\nabla_{\boldsymbol{\theta}} G_{\boldsymbol{\theta}^*}(E(\mathbf{x}))^T \cdot \nabla_{\boldsymbol{\theta}} G_{\boldsymbol{\theta}^*}(E(\mathbf{x}))] + f'(0) \mathbb{E}_{p_{\text{prior}}(\mathbf{z})} [\nabla_{\boldsymbol{\theta}} G_{\boldsymbol{\theta}^*}(\mathbf{z})^T \cdot \nabla_{\mathbf{x}}^2 D_{\boldsymbol{\psi}}(G_{\boldsymbol{\theta}^*}(\mathbf{z})) \cdot \nabla_{\boldsymbol{\theta}} G_{\boldsymbol{\theta}^*}(\mathbf{z})]. \end{aligned}$$

To compute  $K_{DG}$ , we first derive  $\nabla_{\boldsymbol{\theta}} \mathcal{L}$  from Eq. (18) as

$$\nabla_{\boldsymbol{\theta}} \mathcal{L}(\boldsymbol{\theta}, \boldsymbol{\psi}) = -2\eta \mathbb{E}_{p_{\text{data}}(\mathbf{x})} [\langle \mathbf{x} - G_{\boldsymbol{\theta}}(E(\mathbf{x})), \nabla_{\boldsymbol{\theta}} G_{\boldsymbol{\theta}}(E(\mathbf{x})) \rangle] + \nabla_{\boldsymbol{\theta}} \mathbb{E}_{p_{G_{\boldsymbol{\theta}}(\mathbf{x})}} [f(-D_{\boldsymbol{\psi}}(\mathbf{x}))].$$

Thus, we can compute

$$\nabla_{\boldsymbol{\theta}, \boldsymbol{\psi}}^2 \mathcal{L}(\boldsymbol{\theta}, \boldsymbol{\psi}) = -\nabla_{\boldsymbol{\theta}} \mathbb{E}_{p_{G_{\boldsymbol{\theta}}}(\mathbf{x})} [f'(-D_{\boldsymbol{\psi}}(\mathbf{x})) \cdot \nabla_{\boldsymbol{\psi}} D_{\boldsymbol{\psi}}(\mathbf{x})],$$

and hence,

$$K_{DG} = \nabla_{\boldsymbol{\theta}, \boldsymbol{\psi}}^2 \mathcal{L}(\boldsymbol{\theta}^*, \boldsymbol{\psi}^*) = -f'(0) \nabla_{\boldsymbol{\theta}} \mathbb{E}_{p_{G_{\boldsymbol{\theta}^*}}(\mathbf{x})} [\nabla_{\boldsymbol{\psi}} D_{\boldsymbol{\psi}^*}(\mathbf{x})] \Big|_{\boldsymbol{\theta}=\boldsymbol{\theta}^*}.$$

To compute  $K_{DD}$ , we can obtain from Eq. (19) that

$$\begin{aligned} \nabla_{\boldsymbol{\psi}}^2 \mathcal{L}(\boldsymbol{\theta}, \boldsymbol{\psi}) &= \mathbb{E}_{p_{\text{data}}(\mathbf{x})} [f''(D_{\boldsymbol{\psi}}(\mathbf{x})) \nabla_{\boldsymbol{\psi}} D_{\boldsymbol{\psi}}(\mathbf{x}) \cdot \nabla_{\boldsymbol{\psi}} D_{\boldsymbol{\psi}}(\mathbf{x})^T] \\ &\quad + \mathbb{E}_{p_{G_{\boldsymbol{\theta}}}(\mathbf{x})} [f''(-D_{\boldsymbol{\psi}}(\mathbf{x})) \nabla_{\boldsymbol{\psi}} D_{\boldsymbol{\psi}}(\mathbf{x}) \cdot \nabla_{\boldsymbol{\psi}} D_{\boldsymbol{\psi}}(\mathbf{x})^T] \\ &\quad + \mathbb{E}_{p_{\text{data}}(\mathbf{x})} [f'(D_{\boldsymbol{\psi}}(\mathbf{x})) \nabla_{\boldsymbol{\psi}}^2 D_{\boldsymbol{\psi}}(\mathbf{x})] - \mathbb{E}_{p_{G_{\boldsymbol{\theta}}}(\mathbf{x})} [f'(-D_{\boldsymbol{\psi}}(\mathbf{x})) \nabla_{\boldsymbol{\psi}}^2 D_{\boldsymbol{\psi}}(\mathbf{x})]. \end{aligned}$$

Hence, by using Assumption III-1 (ii) and (iii), we get

$$K_{DD} = \nabla_{\boldsymbol{\psi}}^2 \mathcal{L}(\boldsymbol{\theta}^*, \boldsymbol{\psi}^*) = 2f''(0) \mathbb{E}_{p_{\text{data}}(\mathbf{x})} [\nabla_{\boldsymbol{\psi}} D_{\boldsymbol{\psi}^*}(\mathbf{x}) \cdot \nabla_{\boldsymbol{\psi}} D_{\boldsymbol{\psi}^*}(\mathbf{x})^T].$$

■

We consider the following two sets

$$\begin{aligned} \mathcal{M}_G &:= \{\boldsymbol{\theta} \mid p_{\boldsymbol{\theta}} = p_{\text{data}}, \mathbf{x} = G_{\boldsymbol{\theta}}(E(\mathbf{x})) \text{ for a.e. } \mathbf{x} \in \text{supp}(p_{\text{data}})\} \\ \mathcal{M}_D &:= \{\boldsymbol{\psi} \mid S(\boldsymbol{\psi}) = 0\}, \end{aligned}$$

where  $S(\boldsymbol{\psi}) := \mathbb{E}_{p_{\text{data}}(\mathbf{x})} [|D_{\boldsymbol{\psi}}(\mathbf{x})|^2 + \|\nabla_{\mathbf{x}} D_{\boldsymbol{\psi}}(\mathbf{x})\|_2^2]$ . Also, we let  $\mathcal{T}_{\boldsymbol{\psi}^*} \mathcal{M}_D$  denote the tangent space of  $\mathcal{M}_D$  at  $\boldsymbol{\psi}^*$ .

**Assumption III-2.** (i) The second continuously differentiable function  $f: \mathbb{R} \rightarrow \mathbb{R}$  satisfies:  $f'(0) > 0$  and  $f''(0) < 0$ .

(ii) There is a  $\delta > 0$  so that  $\mathcal{M}_G \cap \mathbb{B}_{\delta}(\boldsymbol{\theta}^*)$  and  $\mathcal{M}_D \cap \mathbb{B}_{\delta}(\boldsymbol{\psi}^*)$  are  $\mathcal{C}^1$  manifolds.

(iii)  $\nabla_{\boldsymbol{\theta}} G_{\boldsymbol{\theta}^*}(E(\mathbf{x}))^T \cdot \nabla_{\boldsymbol{\theta}} G_{\boldsymbol{\theta}^*}(E(\mathbf{x}))$  is positive definite, for all  $\mathbf{x} \in \text{supp}(p_{\text{data}})$ .

(iv)  $\partial_{\mathbf{w}} h(\boldsymbol{\psi}^*) \neq 0$  for any  $\mathbf{w} \notin \mathcal{T}_{\boldsymbol{\psi}^*} \mathcal{M}_D$ , where  $h(\boldsymbol{\psi}) := \nabla_{\boldsymbol{\theta}} \mathbb{E}_{p_{G_{\boldsymbol{\theta}}}(\mathbf{x})} [D_{\boldsymbol{\psi}}(\mathbf{x})] \Big|_{\boldsymbol{\theta}=\boldsymbol{\theta}^*}$ .

(v)  $\mathbf{w}^T \nabla_{\mathbf{x}}^2 D_{\boldsymbol{\psi}^*}(\mathbf{x}) \mathbf{w} \geq 0$ , for all  $\mathbf{w} \notin \mathcal{T}_{\boldsymbol{\theta}^*} \mathcal{M}_G$  and  $\mathbf{x} \in \text{supp}(p_{\text{data}})$ .

*Remark.* Two special cases are either (v-1)  $\nabla_{\mathbf{x}}^2 D_{\boldsymbol{\psi}^*}(\mathbf{x}) = 0$  for  $\mathbf{x} \in \text{supp}(p_{\text{data}})$ , or (v-2)  $\mathbf{w}^T \nabla_{\mathbf{x}}^2 D_{\boldsymbol{\psi}^*}(\mathbf{x}) \mathbf{w} > 0$ , for all  $\mathbf{w} \notin \mathcal{T}_{\boldsymbol{\theta}^*} \mathcal{M}_G$  and  $\mathbf{x} \in \text{supp}(p_{\text{data}})$ .

**Theorem B.9.** Suppose that Assumptions III-1 and III-2 hold for an equilibrium  $(\boldsymbol{\theta}^*, \boldsymbol{\psi}^*)$  and  $\eta > 0$  is sufficiently large. Then the alternative gradient descent iteration  $\mathcal{F}_h$  described in Section B.3.2 is locally convergent on  $\mathcal{M}_G \times \mathcal{M}_D$  for a sufficiently small learning rate  $h > 0$ .

**Proof of Theorem B.9.** The argument is motivated by [27]. We notice that  $\mathcal{M}_G \times \mathcal{M}_D$  is a subset of all equilibria of the operators  $\mathcal{F}_h$  (or  $\mathbf{v}(\boldsymbol{\theta}, \boldsymbol{\psi})$ ). This is because that for any  $(\boldsymbol{\theta}, \boldsymbol{\psi}) \in \mathcal{M}_G \times \mathcal{M}_D$ , we have  $p_{\boldsymbol{\theta}} = p_{\text{data}}$ ,  $\mathbf{x} = G_{\boldsymbol{\theta}}(E(\mathbf{x}))$ ,  $D_{\boldsymbol{\psi}}(\mathbf{x}) = 0$ , and  $\nabla_{\mathbf{x}} D_{\boldsymbol{\psi}}(\mathbf{x}) = \mathbf{0}$  for  $\mathbf{x} \in \text{supp}(p_{\text{data}})$ . From Eqs. (20) and (21), we then can obtain  $\nabla_{\boldsymbol{\theta}} \mathcal{L}(\boldsymbol{\theta}, \boldsymbol{\psi}) = \nabla_{\boldsymbol{\psi}} \mathcal{L}(\boldsymbol{\theta}, \boldsymbol{\psi}) = 0$ , meaning  $(\boldsymbol{\theta}, \boldsymbol{\psi})$  is an equilibrium.

Now, we show that the alternating gradient descent converges locally on  $\mathcal{M}_G \times \mathcal{M}_D$  by verifying Lemma B.8 is fulfilled, and hence, Lemma B.7 can be applied. Let  $(\boldsymbol{\theta}^*, \boldsymbol{\psi}^*) \in \mathcal{M}_G \times \mathcal{M}_D$ . There is a  $\mathcal{C}^1$ -diffeomorphism  $\Psi$  that transforms a neighborhood of  $(\boldsymbol{\theta}^*, \boldsymbol{\psi}^*)$  onto an open set in  $\mathbb{R}^{(N+M)}$  due to Assumption III-2 (ii). More precisely, we can compute the relation of  $\mathcal{F}_h$  and  $\mathbf{v}$  after the  $\Psi$ -reparametrization. Let  $\boldsymbol{\zeta} := \Psi(\boldsymbol{\theta}, \boldsymbol{\psi})$ , and

$$\begin{aligned} \mathcal{F}_h^{\Psi}(\boldsymbol{\zeta}) &:= \Psi \circ \mathcal{F}_h \circ \Psi^{-1}(\boldsymbol{\zeta}) \\ \mathbf{v}^{\Psi}(\boldsymbol{\zeta}) &:= \Psi'(\boldsymbol{\theta}, \boldsymbol{\psi}) \cdot (\mathbf{v} \circ \Psi^{-1}(\boldsymbol{\zeta})). \end{aligned}$$

Then

$$\nabla_{\boldsymbol{\zeta}} \mathcal{F}_h^{\Psi}(\boldsymbol{\zeta}^*) = \nabla_{\boldsymbol{\theta}, \boldsymbol{\psi}} \Psi(\boldsymbol{\theta}^*, \boldsymbol{\psi}^*) \cdot \nabla_{\boldsymbol{\theta}, \boldsymbol{\psi}} \mathcal{F}_h(\boldsymbol{\theta}^*, \boldsymbol{\psi}^*) \cdot \nabla_{\boldsymbol{\theta}, \boldsymbol{\psi}} \Psi(\boldsymbol{\theta}^*, \boldsymbol{\psi}^*)^{-1}$$

$$\nabla_{\zeta} \mathbf{v}^{\Psi}(\zeta^*) = \nabla_{\theta, \psi} \Psi(\theta^*, \psi^*) \cdot \nabla_{\theta, \psi} \mathbf{v}(\theta^*, \psi^*) \cdot \nabla_{\theta, \psi} \Psi(\theta^*, \psi^*)^{-1}.$$

We remark that similar matrices have identical ranks and spectrum. Therefore, without loss of the generality, we can assume that  $(\theta^*, \psi^*) = (\mathbf{0}_N, \mathbf{0}_M) \in \mathbb{R}^N \times \mathbb{R}^M$ , and

$$\begin{aligned} \mathcal{M}_G &= \mathcal{T}_{\theta^*} \mathcal{M}_G = \{0\}^{N_G} \times \mathbb{R}^{N-N_G} \\ \mathcal{M}_D &= \mathcal{T}_{\psi^*} \mathcal{M}_D = \{0\}^{M_D} \times \mathbb{R}^{M-M_D}. \end{aligned}$$

We write the new parameterizations as  $\theta := (\mathbf{v}_G, \boldsymbol{\omega}_G) \in \mathbb{R}^{N_G} \times \mathbb{R}^{N-N_G}$  and  $\psi := (\mathbf{v}_D, \boldsymbol{\omega}_D) \in \mathbb{R}^{M_D} \times \mathbb{R}^{M-M_D}$ . For simplicity, we write  $\mathbf{v}(\theta, \psi) := \mathbf{v}(\mathbf{v}_G, \boldsymbol{\omega}_G, \mathbf{v}_D, \boldsymbol{\omega}_D)$ . To apply Lemma B.7, we now aim to show that  $\nabla_{(\mathbf{v}_G, \mathbf{v}_D)} \mathbf{v}(\theta^*, \psi^*)$  only admits eigenvalues with negative real parts. From Lemma B.8,

$$\nabla_{(\mathbf{v}_G, \mathbf{v}_D)} \mathbf{v}(\theta^*, \psi^*) = \begin{bmatrix} \hat{K}_{GG} & -\hat{K}_{DG}^T \\ \hat{K}_{DG} & \hat{K}_{DD} \end{bmatrix}.$$

Here,  $\hat{K}_{GG}$ ,  $\hat{K}_{DG}$ , and  $\hat{K}_{DD}$  represent submatrices of  $K_{GG}$ ,  $K_{DG}$ , and  $K_{DD}$ , respectively, with coordinates  $(\mathbf{v}_G, \mathbf{v}_D)$ , indicating the Jacobian of  $\mathbf{v}$  with derivatives taken along the  $\mathbf{v}_G$  and  $\mathbf{v}_D$  directions.

First of all, we show that  $K_{DD}$  is generally negative semi-definite. Let  $\boldsymbol{\xi} \in \mathbb{R}^{(N+M)}$  be any vector. Then

$$\begin{aligned} \boldsymbol{\xi}^T K_{DD} \boldsymbol{\xi} &= 2f''(0) \mathbb{E}_{p_{\text{data}}(\mathbf{x})} [\boldsymbol{\xi}^T \nabla_{\psi} D_{\psi^*}(\mathbf{x}) \cdot \nabla_{\psi} D_{\psi^*}(\mathbf{x})^T \boldsymbol{\xi}] \\ &= 2f''(0) \mathbb{E}_{p_{\text{data}}(\mathbf{x})} [(\nabla_{\psi} D_{\psi^*}(\mathbf{x})^T \boldsymbol{\xi})^T \cdot \nabla_{\psi} D_{\psi^*}(\mathbf{x})^T \boldsymbol{\xi}] \leq 0, \end{aligned}$$

because  $f''(0) < 0$  from Assumption III-2 (i). Thus, for any  $\hat{\boldsymbol{\xi}}_G \in \mathbb{R}^{N_G}$  and  $\hat{\boldsymbol{\xi}}_D \in \mathbb{R}^{M_D}$  if we consider  $\hat{\boldsymbol{\xi}} := (\hat{\boldsymbol{\xi}}_G, \hat{\boldsymbol{\xi}}_D)$  in  $(\mathbf{v}_G, \mathbf{v}_D)$ -coordinate,

$$\hat{\boldsymbol{\xi}}^T \hat{K}_{DD} \hat{\boldsymbol{\xi}} = \boldsymbol{\xi}^T K_{DD} \boldsymbol{\xi} \leq 0,$$

where  $\boldsymbol{\xi} := (\hat{\boldsymbol{\xi}}_G, \mathbf{0}_{N-N_G}, \hat{\boldsymbol{\xi}}_D, \mathbf{0}_{M-M_D}) \in \mathbb{R}^{(N+M)}$ .

Next, we demonstrate that  $\hat{K}_{DG}$  is full rank. We observe that  $\hat{\boldsymbol{\xi}}_D \neq 0$  if and only if  $\boldsymbol{\xi} \notin \mathcal{T}_{\psi^*} \mathcal{M}_D$ . Then, according to Assumption III-2 (iv), we deduce that if  $\hat{\boldsymbol{\xi}}_D \neq 0$

$$K_{DG} \boldsymbol{\xi} = -f'(0) \nabla_{\theta} \mathbb{E}_{p_{G\theta^*}(\mathbf{x})} [\nabla_{\psi} D_{\psi^*}(\mathbf{x}) \cdot \boldsymbol{\xi}] \Big|_{\theta=\theta^*} = -f'(0) \partial_{\boldsymbol{\xi}} h(\psi^*) \neq 0.$$

The elements of  $K_{DG} \boldsymbol{\xi}$  corresponding to the  $\mathbf{v}_D$ -coordinates are represented by  $\hat{K}_{DG} \hat{\boldsymbol{\xi}}_D$ , while those corresponding to the  $\boldsymbol{\omega}_D$ -coordinates are 0. Therefore, we conclude that  $\hat{K}_{DG} \hat{\boldsymbol{\xi}}_D \neq 0$ . Consequently, by the rank-nullity theorem,  $\hat{K}_{DG}$  is full-rank.

Finally, by using similar arguments by selecting  $(\mathbf{v}_G, \mathbf{v}_D)$ -coordinate, without loss of generality, we only need to show  $K_{GG}$  is negative definite. By applying Assumption III-2 (i) and (v), the following lemma concludes that if  $\eta > 0$  is sufficiently large, we can conclude the negative definiteness of  $\nabla_{\theta}^2 \mathcal{L}(\theta^*, \psi^*)$  under Assumption III-2 (v-2).

**Lemma B.10.** *Let  $\mathbf{A}$  be positive definite, and  $\mathbf{B}$  be positive semi-definite. Then there is a  $\eta_{\min} > 0$  so that  $-\eta \mathbf{A} + \mathbf{B}$  is negative definite for all  $\eta > \eta_{\min}$ .*

The lemma holds because, for positive (semi-) definite matrix  $\mathbf{X}$ , we generally have

$$\lambda_{\max}(\mathbf{X}) \|\mathbf{w}\|^2 \geq \mathbf{w}^T \mathbf{X} \mathbf{w} \geq \lambda_{\min}(\mathbf{X}) \|\mathbf{w}\|^2,$$

for all  $\mathbf{w}$ . Here,  $\lambda_{\max}(\mathbf{X})$  and  $\lambda_{\min}(\mathbf{X})$  denote the maximum and minimum eigenvalues of  $\mathbf{X}$ , respectively. Thus if select  $\eta > \frac{\lambda_{\max}(\mathbf{B})}{\lambda_{\min}(\mathbf{A})}$ , then for any  $\mathbf{w} \neq \mathbf{0}$ , we have

$$\mathbf{w}^T (-\eta \mathbf{A} + \mathbf{B}) \mathbf{w} = -\eta \mathbf{w}^T \mathbf{A} \mathbf{w} + \mathbf{w}^T \mathbf{B} \mathbf{w} \leq (-\eta \lambda_{\min}(\mathbf{A}) + \lambda_{\max}(\mathbf{B})) \|\mathbf{w}\|_2^2 < 0.$$

By applying Lemma B.6, we know that  $\nabla_{(\mathbf{v}_G, \mathbf{v}_D)} \mathbf{v}(\theta^*, \psi^*)$  only has eigenvalues with negative real parts. Therefore, with a sufficiently small learning rate  $h > 0$ , Lemma B.7 guarantees the locally convergence of  $\mathcal{F}_h$  on  $\mathcal{M}_G \times \mathcal{M}_D$ . ■



### B.3.4 Literature on Stability Analysis of Adversarial Training

Studying the stability of GAN training from a dynamical systems perspective has been a popular approach [76, 28, 27, 77–80]. Generally, proving or disproving whether adversarial training is stable is challenging. However, [27] provides an example (Dirac-GAN) showing that, in general, GANs are not stable unless additional conditions are imposed.

As a result, researchers have explored additional conditions to stabilize GAN training. Essentially, the goal is to impose extra regularizations on the GAN loss  $\mathcal{L}_{\text{GAN}}(\boldsymbol{\theta}, \boldsymbol{\psi}) := \mathbb{E}_{p_{\text{data}}(\mathbf{x})} [f(D_{\boldsymbol{\psi}}(\mathbf{x}))] + \mathbb{E}_{p_{G_{\boldsymbol{\theta}}}(\mathbf{x})} [f(-D_{\boldsymbol{\psi}}(\mathbf{x}))]$ , or its velocity field  $\mathbf{v}_{\text{GAN}}(\boldsymbol{\theta}, \boldsymbol{\psi}) := \begin{bmatrix} -\nabla_{\boldsymbol{\theta}} \mathcal{L}_{\text{GAN}}(\boldsymbol{\theta}, \boldsymbol{\psi}) \\ \nabla_{\boldsymbol{\psi}} \mathcal{L}_{\text{GAN}}(\boldsymbol{\theta}, \boldsymbol{\psi}) \end{bmatrix}$  to ensure that the resulting Jacobian is Hurwitz. To elaborate further, we revisit the Jacobian  $\mathcal{J}_{\text{GAN}}$  of the vanilla GAN, given by  $\mathbf{v}_{\text{GAN}}(\boldsymbol{\theta}, \boldsymbol{\psi})$ :

$$\mathcal{J}_{\text{GAN}}(\boldsymbol{\theta}, \boldsymbol{\psi}) := \begin{bmatrix} -\nabla_{\boldsymbol{\theta}}^2 \mathcal{L}_{\text{GAN}}(\boldsymbol{\theta}, \boldsymbol{\psi}) & -\nabla_{\boldsymbol{\theta}, \boldsymbol{\psi}}^2 \mathcal{L}_{\text{GAN}}(\boldsymbol{\theta}, \boldsymbol{\psi}) \\ \nabla_{\boldsymbol{\theta}, \boldsymbol{\psi}}^2 \mathcal{L}_{\text{GAN}}(\boldsymbol{\theta}, \boldsymbol{\psi}) & \nabla_{\boldsymbol{\psi}}^2 \mathcal{L}_{\text{GAN}}(\boldsymbol{\theta}, \boldsymbol{\psi}) \end{bmatrix} = \begin{bmatrix} K_{GG} & -K_{DG}^T \\ K_{DG} & K_{DD} \end{bmatrix}.$$

Here, we slightly abuse the notation from Section B.3.3 by using  $K_{ij}$ ,  $i, j \in \{D, G\}$ , to denote the corresponding components in  $\mathcal{J}_{\text{GAN}}$ . By similar argument of Lemma B.8, we can obtain (indeed,  $\eta = 0$  in Lemma B.8) that

$$\begin{aligned} K_{GG} &= f'(0) \mathbb{E}_{p_{\text{prior}}(\mathbf{z})} [\nabla_{\boldsymbol{\theta}} G_{\boldsymbol{\theta}^*}(\mathbf{z})^T \cdot \nabla_{\mathbf{x}}^2 D_{\boldsymbol{\psi}^*}(G_{\boldsymbol{\theta}^*}(\mathbf{z})) \cdot \nabla_{\boldsymbol{\theta}} G_{\boldsymbol{\theta}^*}(\mathbf{z})], \\ K_{DG} &= -f'(0) \nabla_{\boldsymbol{\theta}} \mathbb{E}_{p_{G_{\boldsymbol{\theta}}}(\mathbf{x})} [\nabla_{\boldsymbol{\psi}} D_{\boldsymbol{\psi}^*}(\mathbf{x})] \Big|_{\boldsymbol{\theta}=\boldsymbol{\theta}^*}, \\ K_{DD} &= 2f''(0) \mathbb{E}_{p_{\text{data}}(\mathbf{x})} [\nabla_{\boldsymbol{\psi}} D_{\boldsymbol{\psi}^*}(\mathbf{x}) \cdot \nabla_{\boldsymbol{\psi}} D_{\boldsymbol{\psi}^*}(\mathbf{x})^T]. \end{aligned}$$

Conceptually [74, 75], if we can ensure that the Jacobian at some equilibrium has only eigenvalues with strictly negative real parts, then the gradient descent iteration of  $\mathcal{L}_{\text{GAN}}$  is asymptotically stable at that equilibrium. Therefore, the objective of many studies [76, 28, 27, 80] is to find conditions to verify Lemma B.6. We focus on discussing the conditions for  $K_{GG}$  and  $K_{DD}$  to be negative (semi-)definite, as this distinguishes PaGoDA’s Theorem B.9 from the existing literature.

Under Assumption III-2 (i) that  $f''(0) < 0$ , it is worth noting that  $K_{DD}$  is generally negative semi-definite without additional conditions. Hence, studies [76, 28, 27] attempted to impose additional regularizers on  $\mathcal{J}_{\text{GAN}}$  or  $\mathbf{v}_{\text{GAN}}$  to ensure that either  $K_{DD}$  is negative definite (as in [28, 27]) or  $K_{GG}$  is negative definite (as in [27]). In Table 8, we provide a comparison of the various assumptions, at a high-level, drawn from the literature.

We emphasize that PaGoDA does not require  $\nabla_{\mathbf{x}}^2 D_{\boldsymbol{\psi}^*}(\mathbf{x})$  to be strictly positive definite, thanks to PaGoDA’s reconstruction loss. Specifically, it accommodates the scenario where  $\nabla_{\mathbf{x}}^2 D_{\boldsymbol{\psi}^*}(\mathbf{x}) = 0$  on  $\text{supp}(p_{\text{data}})$ . It’s noteworthy that this capability enables PaGoDA to address cases where the instability of GAN is demonstrated, as exemplified by examples provided by [27].

Table 8: Comparison of various assumptions on stability analysis.

Method	$K_{GG}$	$K_{DD}$
[28]’s Vanilla GAN	Both $p_{\text{data}}$ and $p_{\theta}$ covers the whole space $\mathbb{R}^D$ .	Additional technical assumptions (difficult to verify).
[27]’s Vanilla GAN	<ul style="list-style-type: none"> <li>• <math>D_{\psi^*}(\mathbf{x}) = \nabla_{\mathbf{x}} D_{\psi^*}(\mathbf{x}) = 0</math> on <math>\text{supp}(p_{\text{data}})</math>.</li> <li>• <math>\nabla_{\mathbf{x}}^2 D_{\psi^*}(\mathbf{x})</math> positive definite.</li> </ul> <p>This implies <math>K_{GG}</math> is negative definite.</p>	No further assumptions.
[27]’s Regularized GAN	<ul style="list-style-type: none"> <li>• <math>D_{\psi^*}(\mathbf{x}) = \nabla_{\mathbf{x}} D_{\psi^*}(\mathbf{x}) = 0</math> on <math>\text{supp}(p_{\text{data}})</math>.</li> <li>• <math>\nabla_{\mathbf{x}}^2 D_{\psi^*}(\mathbf{x}) = 0</math> on <math>\text{supp}(p_{\text{data}})</math>.</li> </ul> <p>This simply implies <math>K_{GG} = 0</math>.</p>	By introducing a regularizer to modify the vector field $\mathbf{v}$ and obtaining a new vector field $\tilde{\mathbf{v}}$ , they can determine an $L_{DD}$ so that $\tilde{K}_{DD} := K_{DD} - L_{DD}$ is negative definite. Therefore, it is not vanilla GAN anymore.
PaGoDA	<ul style="list-style-type: none"> <li>• <math>D_{\psi^*}(\mathbf{x}) = \nabla_{\mathbf{x}} D_{\psi^*}(\mathbf{x}) = 0</math> on <math>\text{supp}(p_{\text{data}})</math>.</li> <li>• <math>\nabla_{\mathbf{x}}^2 D_{\psi^*}(\mathbf{x})</math> just need to be positive semi-definite on <math>\text{supp}(p_{\text{data}})</math>.</li> </ul> <p>Then with <math>\eta &gt; 0</math> chosen to be sufficiently large in PaGoDA, <math>K_{GG}</math> is negative definite.</p>	No further assumptions.